Journal of Structural Geology 30 (2008) 1202–1217

Contents lists available at ScienceDirect

Journal of Structural Geology

journal homepage: www.elsevier.com/locate/jsg

Multiple injections of magmas along a Hercynian mid-crustal shear zone (Sila Massif, Calabria, Italy)

Domenico Liotta [a,*], Alfredo Caggianelli [b], Jörn H. Kruhl [c], Vincenzo Festa [b], Giacomo Prosser [d], Antonio Langone [e]

[a] Dipartimento di Geologia e Geofisica, Università di Bari, Campus universitario, Via Orabona 4, 70125 Bari, Italy
[b] Dipartimento Geomineralogico, Università di Bari, Bari, Italy
[c] Tectonics and Material Fabrics Section, Technische Universität München, Munich, Germany
[d] Dipartimento di Scienze Geologiche, Università della Basilicata, Potenza, Italy
[e] Dipartimento di Scienze della Terra e Geologico-Ambientali, Università di Bologna, Bologna, Italy

ARTICLE INFO

Article history:
Received 5 November 2007
Received in revised form 9 April 2008
Accepted 15 April 2008
Available online 29 April 2008

Keywords:
Magma emplacement
Shear zone
Late Hercynian
Calabria

ABSTRACT

Syn-tectonic late-Hercynian granitoids, emplaced at mid-crustal level through multiple dyke injections, are well-exposed in a ~1 km-long section, in the southern Sila Massif (Calabria, Italy). The fieldwork study permitted us to reconstruct the following order of emplacement: (i) granodiorites with euhedral Kfs megacrystals (Grd1, in the main text) and heterogranular granodiorites with coarse rounded Pl and Kfs in a fine-grained biotite-rich matrix (Grd2); (ii) granodiorites with a nearly homogeneous grain size (Grd3); (iii) tonalite; and (iv) granite. Both in the wall-rock, represented by migmatitic paragneisses, and in the deformed granitoids the foliation attitude is substantially homogeneous, striking about N140 with a dip of 50–60° to the NE. The magmatic lineation is defined by the preferred alignment of euhedral feldspars, parallel to the mineral lineation observed in the host rocks. Micro- and meso-structural analyses indicate that foliation evolved from melt-present to solid-state conditions. Feldspar tiling, S/C structures, σ-type structures, *c*-axis quartz orientations commonly suggest a top-to-the-west sense of shear during magma injection and deformation under decreasing temperatures. Age of magma emplacement is constrained by U/Pb datings at 304–300 Ma, coeval with the regional metamorphic peak. Foliated granitoids and wall-rock are intruded by poorly foliated Hbl-gabbro and, finally, by undeformed leucogranite, pegmatite and felsic porphyritic dykes. New U/Pb datings of the last intrusion event indicate an age of emplacement of 281 ± 8 Ma, providing a minimum estimate for the end of the shear strain at mid-crustal level.

1. Introduction

Large-scale shear zones in the continental crust can easily become preferred channels for the migration and ascent of granitoid magmas (Hollister and Crawford, 1986; D'Lemos et al., 1992; Neves et al., 1996). If the supply of magmas is continuous, thermal softening is expected, enhancing ductile deformation and localisation of shearing, in both contractional and extensional domains (Hutton, 1982, 1988). Other factors being equal (i.e.: composition, strain rate or velocity of magma supply), syn-kinematic granitoids record deformation if their cooling rate is sufficiently slow to permit the development of deformation fabrics during crystallisation (Paterson et al., 1989). Therefore, syn-kinematic granitoids, cooling at mid- to lower-crust levels, are the best candidates to undergo continuous deformation, from sub-magmatic flow to solid-state conditions (Tribe and D'Lemos, 1996; Vernon, 2000 and references therein).

In these crustal environments, involvement of both mantle- and crust-derived melts is common and hybrid magmas can be generated by mingling/mixing processes (Neves and Vauchez, 1995; Fernandez et al., 1997). By structural and petrologic observations, it is possible to infer the progressive involvement of magmas derived from different sources into the shear zone. Then, dating of the magmatic rocks would also permit to encompass the age of deformation.

In this paper we deal with multiple syn-kinematic injections of magmas within a late-Hercynian mid-crustal shear zone cropping out in the Sila Massif (Figs. 1 and 2) at the boundary between high-grade metamorphic rocks and granitoids. Shear-zone foliation is mainly north-east dipping and kinematic indicators commonly point out a top-to-the-west sense of shear (Festa et al., 2006). We studied a section of this regional shear zone, close to the Mesoraca town, where the relationships between several late-Carboniferous

* Corresponding author. Tel.: +39 080 544 2573; fax: +39 080 544 2625.
E-mail address: d.liotta@geo.uniba.it (D. Liotta).

0191-8141/$ – see front matter © 2008 Elsevier Ltd. All rights reserved.
doi:10.1016/j.jsg.2008.04.005

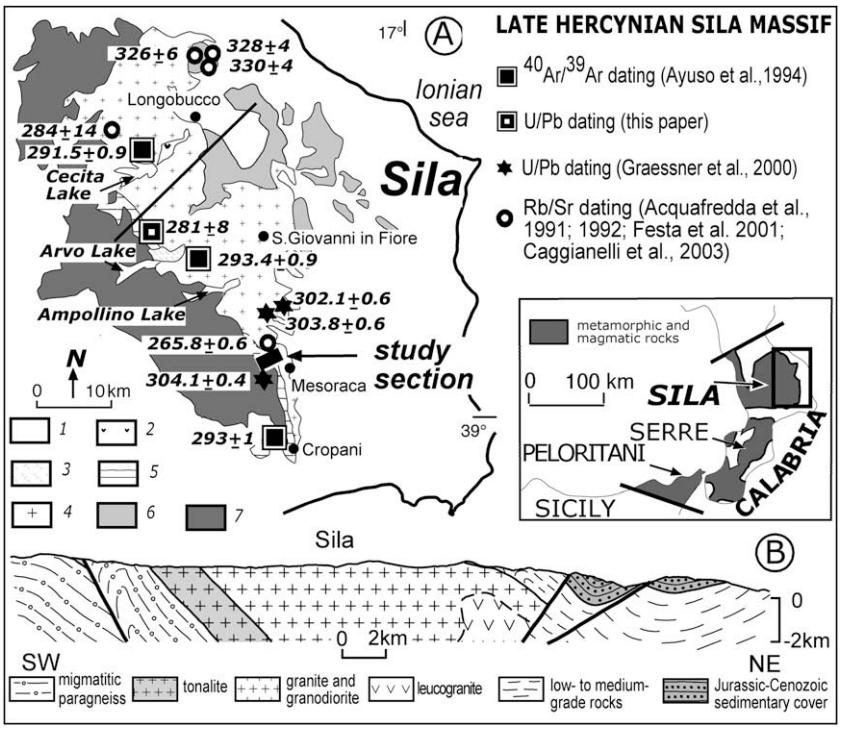

Fig. 1. (A) Sketch map of the late-Hercynian Sila Massif and location of the study section to the north of the Mesoraca village. The main geochronologic datings of the area are also reported. Symbols: (1) Mesozoic to Quaternary sedimentary rocks; (2) leucogranite; (3) gabbro-diorite; (4) metaluminous to strongly peraluminous granite and granodiorite; (5) tonalite; (6) low- to medium-grade metamorphic rocks; (7) high-grade metamorphic rocks. (B) Schematic geological section through the Sila Massif (after Caggianelli et al., 1997; Graessner et al., 2000).

syn- to post-tectonic granitoids (Ayuso et al., 1994; Graessner et al., 2000) can be clearly observed (Fig. 1). Granitoids show calc-alkaline affinity and composition varying from tonalite to two-mica strongly peraluminous leucogranite (Caggianelli and Prosser, 2001 and references therein).

Our results allow to (i) unravel the sequence of intrusions, (ii) recognise continuous deformation from magmatic through high-T to low-T conditions, within the same kinematic framework, and (iii) discuss the tectonic environment for the emplacement of the granitoids in the Sila Massif.

2. Geological setting

The Calabria–Peloritani terrane (Bonardi et al., 2001) builds a curved mountain belt, connecting the NW–SE-trending southern Apennines and the E–W-trending Maghrebide chain of Sicily (Amodio-Morelli et al., 1976). It is a fault-bounded terrane that was involved in the southern Apennines orogeny (Fig. 1). The present structure of the Calabria–Peloritani terrane derives from two main tectonic episodes. The first one occurred during Eocene–Oligocene times and is connected to the collision between the Adria promontory and the European plate (Borsi and Dubois, 1968; Platt and Compagnoni, 1990). The stacking of the Calabria–Peloritani tectonic units is related to this episode (e.g. Amodio-Morelli et al., 1976; Van Dijk et al., 2000 and references therein). The second episode (late-Oligocene to the Present) is related to the south-eastward migration of the Calabria–Peloritani terrane, in relation to retreating subduction of the Ionian oceanic lithosphere and to the opening of the Tyrrhenian oceanic Basin (Dewey et al., 1989; Gueguen et al., 1998 and references therein). During migration, the eastern margin of the Calabria terrane experienced shortening whereas the western margin underwent extension and uplift (Wallis et al., 1993; Thomson, 1994). A consequence of this geological evolution is a regional crustal tilting of about 40–45° (Schenk, 1980; Thomson, 1994; Caggianelli et al., 2000; Festa et al., 2003) that favoured the outcrop of a nearly complete tilted Hercynian crustal section (Dubois, 1976; Schenk, 1980, 1989, 1990). Despite post-Hercynian tectonic events, the original Hercynian structural setting is still preserved in the Sila and Serre massifs (Lorenzoni and Zanettin Lorenzoni, 1983; Atzori et al., 1984; Caggianelli and Prosser, 2001).

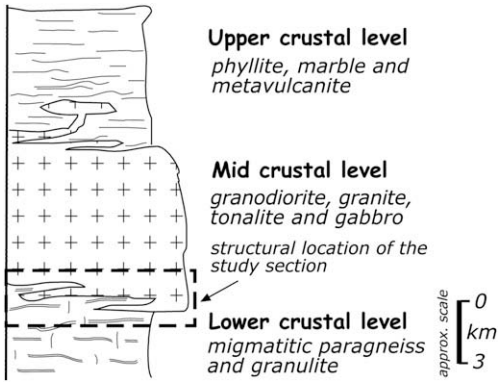

Fig. 2. Schematic lithological column of the late-Hercynian crust cropping out in the Sila Massif. The structural location of the study section is also indicated.

In the Sila area (Fig. 1), the late-Hercynian continental crust is basically composed of high-grade and low-grade Palaeozoic metamorphic rocks, intruded by nearly tabular late-Hercynian granitoids and minor quartz-dioritic to gabbroic bodies (Dubois, 1976; Schenk, 1980; Caggianelli and Prosser, 2001). Granitoids are located between high-grade migmatitic paragneisses (bottom), cropping out to the west, and low-grade metamorphic rocks (top), exposed to the east (Figs. 1 and 2). Their emplacement depths regionally range from 8 to 18 km, with the granitoids in the surrounding of the study area injected at approximately 18 km depth

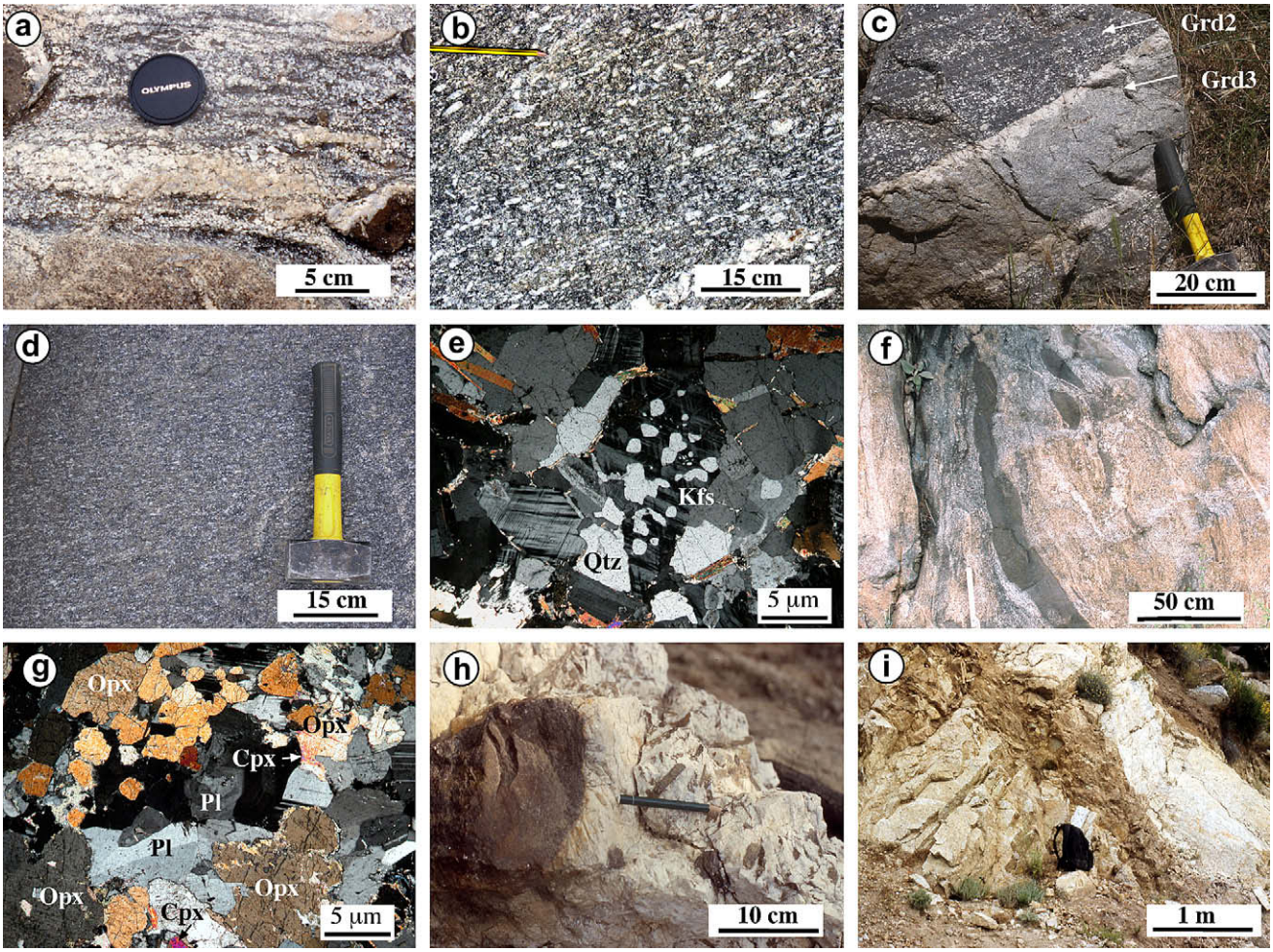

Fig. 3. Outcrop photographs and photomicrographs of the rocks exposed in the study area; outcrop location in Fig. 5a,b. (a) Migmatitic paragneiss injected by a vein departing from the neighbouring granitoids. (b) K-feldspar megacrysts bearing granodiorite, referred to as Grd1 in the text; the strong alignment of euhedreal K-Feldspars indicates that the foliation plane was produced by crystal orientation during magmatic flow; outcrop location in Fig. 5g,h. (c) Equigranular granodiorite (Grd3) intruding the heterogranular granodiorite (Grd2); the boundary is marked by a pegmatite with chilled margins. Geometry of the boundary indicates that Grd3 magma was less viscous than pegmatite magma. (d) Foliated tonalite; outcrop location in Fig. 5f,g. (e) Graphic texture in undeformed leucogranite. (f) Mafic dyke and enclaves parallel to the Grd1 magmatic foliation; outcrop location in Fig. 5h,i. (g) Thin section of norite enclave in the Grd1 granodiorite. (h,i) Undeformed pegmatite and porphyritic dyke, intruding wall-rocks and the previously emplaced granitoids, respectively; outcrop locations in Fig. 5e,f and b,c.

Table 1
Selected chemical analyses of the magmatic rock types involved in the shear deformation

	Amph-gabbro	Dioritic enclave	Tonalite	Granodiorite			Granite	Leucogranite	Pegmatite
				1	2	3			
wt.%									
Sio_2	47.49	56.36	58.25	66.36	64.48	67.42	72.61	74.56	82.73
Tio_2	1.11	0.94	1.21	0.77	1.24	0.83	0.10	0.13	0.03
Al_2O_{3t}	17.91	16.20	17.83	15.14	14.20	15.15	15.34	14.03	9.22
Fe_2O_3	10.38	9.16	7.35	4.59	6.20	4.58	1.44	0.92	0.79
MnO	0.18	0.20	0.11	0.10	0.12	0.10	0.07	0.06	0.09
MgO	7.04	5.13	2.56	1.70	3.47	1.60	0.09	0.08	0.06
CaO	10.98	8.34	5.86	2.64	3.61	1.56	0.86	0.86	0.38
Na_2O	1.86	2.28	2.99	2.75	2.93	2.41	3.10	2.86	1.15
K_2O	1.07	0.71	2.87	5.06	3.00	5.20	5.52	5.87	5.04
P_2O_5	0.13	0.16	0.41	0.40	0.24	0.17	0.21	0.16	0.11
L.O.I.	1.84	0.53	0.56	0.48	0.51	0.98	0.67	0.48	0.41
TOT	99.99	100.01	100.00	99.99	100.00	100.00	100.01	100.01	100.01
A/CNK	0.74	0.82	0.95	1.02	0.97	1.21	1.21	1.11	1.15
ppm									
Rb	47	32	136	185	120	197	179	190	92
Sr	347	208	329	194	191	217	44	108	78
Y	37	33	21	36	38	23	9	5	6
Zr	66	110	418	334	274	263	19	48	18
Nb	7	7	18	19	18	17	16	5	1

(Caggianelli et al., 1997). Age of emplacement for the Sila granitoids spans from 304 to 300 Ma (U/Pb method on zircon and monazite), near synchronously with the peak metamorphism (Graessner et al., 2000). Two peraluminous granites, cropping out in the neighbourhood of the study area, provided monazite and xenotime ages of 303–302 Ma by U/Pb method (Graessner et al., 2000). Datings of tonalite of the study section was performed by $^{40}Ar/^{39}Ar$ method by Ayuso et al. (1994) and resulted in hornblende ages of 293 Ma (Fig. 1), in agreement with the lower closing temperature of hornblende by this geochronologic method, compared to that of monazite by U/Pb method.

Undeformed felsic porphyritic dykes and pegmatites cross-cut all previous rocks and fabrics. An age of 281 ± 8 Ma (see Section 5) has been obtained by U/Pb on zircons for a felsic porphyritic dyke cropping out near Arvo Lake (Fig. 1). A muscovite age of 265 Ma was obtained by Rb/Sr method for a pegmatite (Festa et al., 2001) in a zone located directly northwest of Mesoraca (Fig. 1).

Older ages are from the Devonian metasediments and interlayered metavulcanites of the upper crust (Fig. 1). Here, three ages of the regional metamorphism were estimated by Rb/Sr isochrons of whole-rocks at 326 ± 6 Ma, 328 ± 4 Ma and 330 ± 4 Ma (Acquafredda et al., 1991, 1992).

In the Sila Massif, from bottom to top, high-grade metamorphic rocks are metagabbros, felsic granulites, and migmatitic paragneisses with intervening marbles and metabasites. In the paragneisses, according to Graessner and Schenk (2001), the metamorphic assemblage of biotite–garnet–sillimanite–K-feldspar–cordierite–spinel, indicates peak P-T conditions of 400–600 MPa and 740–770 °C, reached simultaneously with the emplacement of the granitoids, as constrained by geochronologic datings (Graessner et al., 2000). The study section is structurally located at the boundary between granitoids and migmatitic paragneisses (Fig. 2), within a ~5 km thick and ~60 km long regional shear zone (presently under study, with some preliminary data in Festa et al., 2006) extending from the Cropani village to the Cecita Lake area (Fig. 1). In this shear zone, basement rocks and granitoids are involved in a common kinematic framework, dominated by a top-to-the-west sense of shear. An overview of the microstructural features in granitoids suggests shearing during cooling of the intrusive rocks. P-T paths for the wall-rocks are characterised by

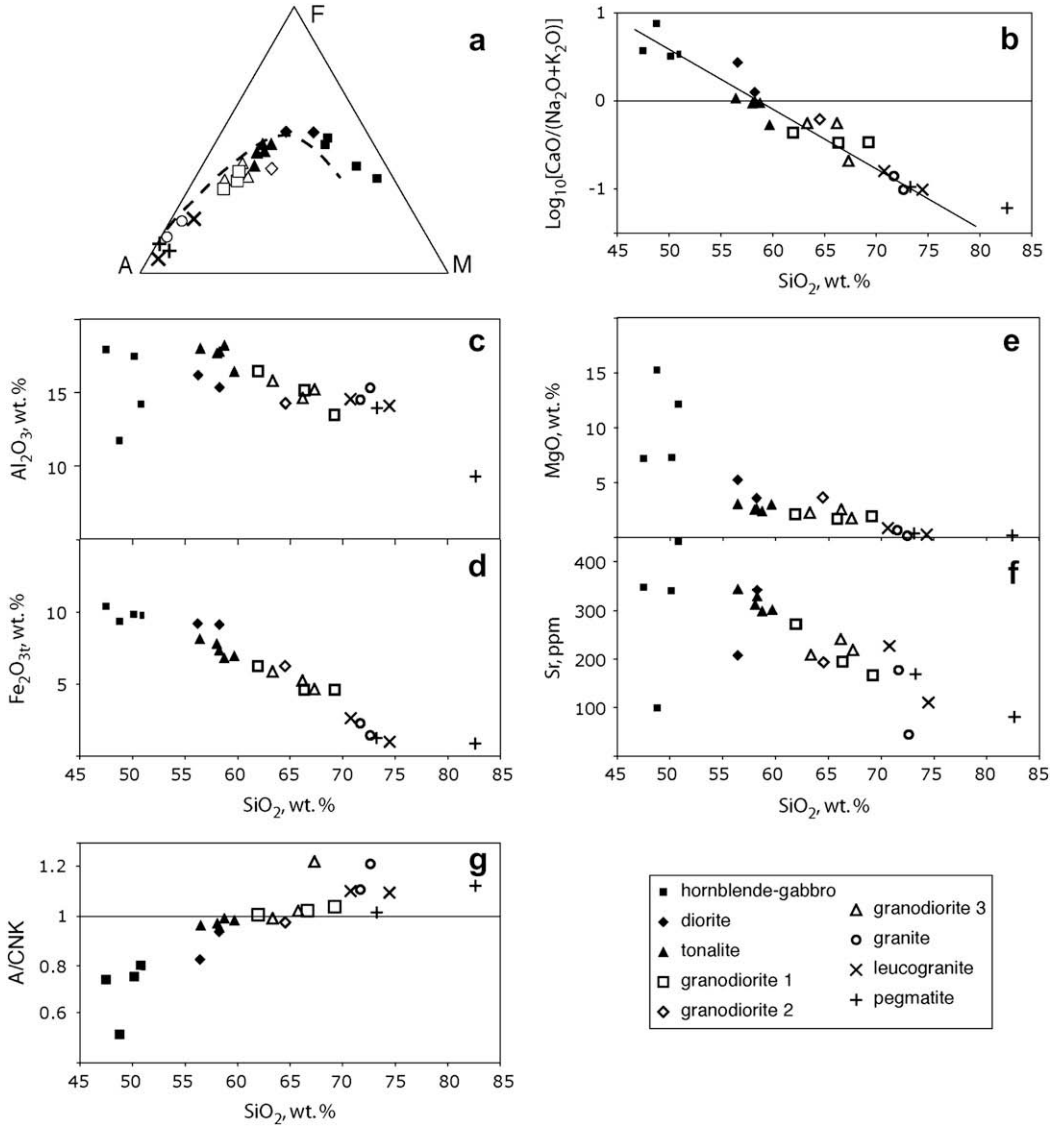

Fig. 4. Overview of the compositional features of the magmatic rocks involved in shear deformation. (a) AFM diagram (dashed curve by Irvine and Baragar, 1971). (b) Alkali–Lime index in the diagram by Brown (1982). (c–f) Harker diagrams for Al_2O_3, Fe_2O_{3t}, MgO and Sr. (g) A/CNK vs. silica diagram (A/CNK = $[Al_2O_3]/\{[CaO] + [Na_2O] + [K_2O]\}$ molecular ratio).

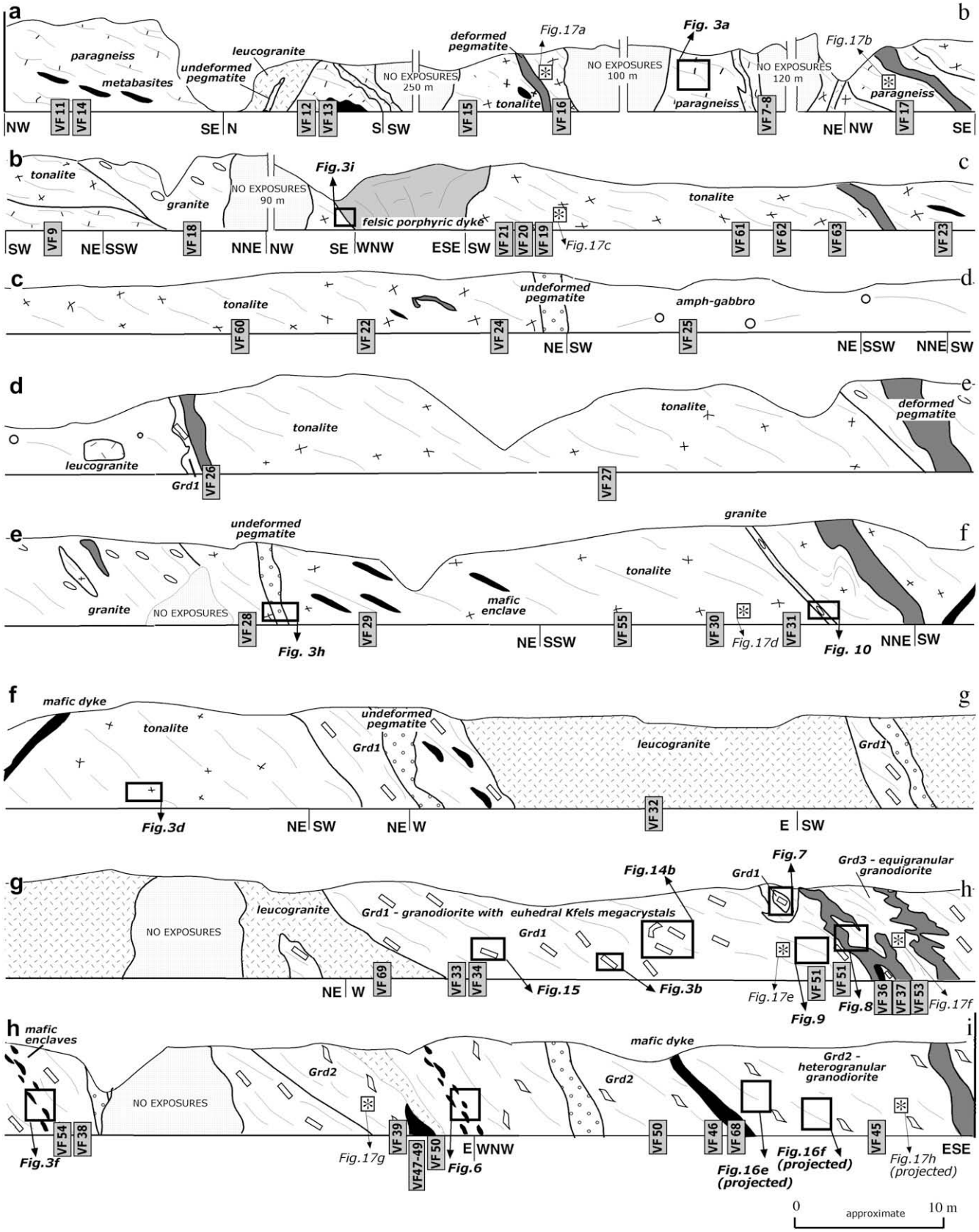

Fig. 5. Geologic profile along the study section; the structural relationships and foliation attitude are displayed. Locations of samples for thin section analysis (from VF7 to VF68), outcrop photographs (squares) and samples for the quartz *c*-axis orientations (stars) are indicated.

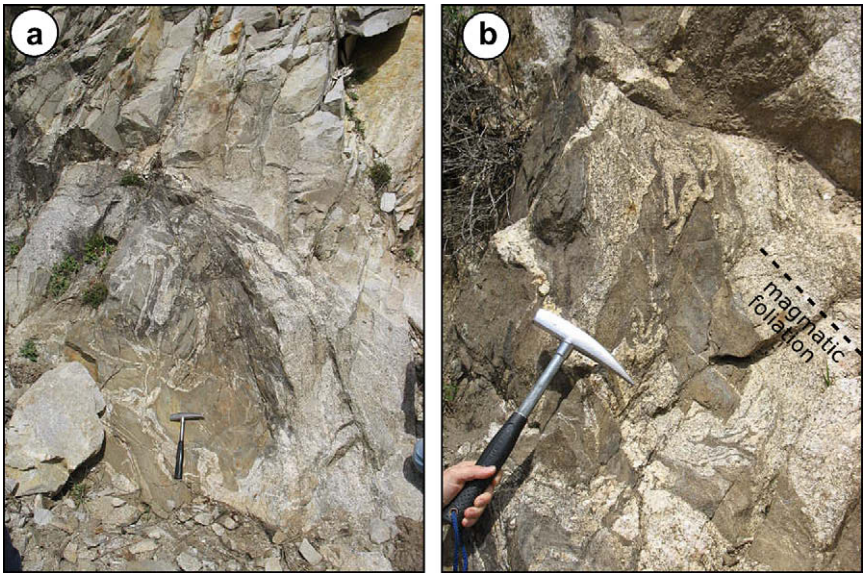

Fig. 6. (a) Disrupted mafic dyke with crenulated margins in the Grd1 granodiorite. (b) Close-up of the previous image, showing an enclave in granodiorite, dismembered from the mafic dyke: granodiorite entrapped in the mafic enclave and vice-versa, indicates mixing/mingling processes; outcrop location in Fig. 5h,i.

a nearly isothermal decompression, compatible with fast exhumation (Graessner and Schenk, 2001).

3. Petrography

In the study section, similarly to other Calabria areas (Rottura et al., 1990), high-grade metamorphic rocks show a migmatitic zone at the contact with the granitoids (Fig. 3a).

Away from the boundary, a wide spectrum of calc-alkaline intrusive rocks crops out over about 1 km perpendicular to strike. These are represented by: granodiorite with euhedral Kfs megacrystals outlining a strong foliation (Grd 1, Fig. 3b); heterogranular foliated dark granodiorite with coarse rounded Pl and Kfs (Fig. 3c) in a fine-grained biotite-rich matrix (Grd2); granodiorite with a nearly equi-granular grain size (Grd3, Fig. 3c); tonalite (Fig. 3d), granite, leucogranite (Fig. 3e), hornblende gabbro, and swarms of mafic enclaves (Fig. 3f) including rare norite xenoliths (Fig. 3g). Granodiorites, tonalite and granite are strongly foliated. Differently, hornblende-gabbro is poorly foliated whereas leucogranite, pegmatite, (Fig. 3h) and felsic porphyritic dykes (Fig. 3i) intruding the host rocks and the previously emplaced granitoids, are undeformed and therefore considered post-tectonic.

3.1. Chemical composition of intrusive rocks

The chemical composition of the intrusive rocks was analysed by Lioy (2006) and is summarised in Table 1. A wide compositional range with silica content comprised between 47.49 wt.% and 74.56 wt.% is observed. Mafic rocks are mostly hornblende gabbros and dioritic enclaves, but noritic compositions are also detected in rare and small xenoliths enclosed in granodiorites.

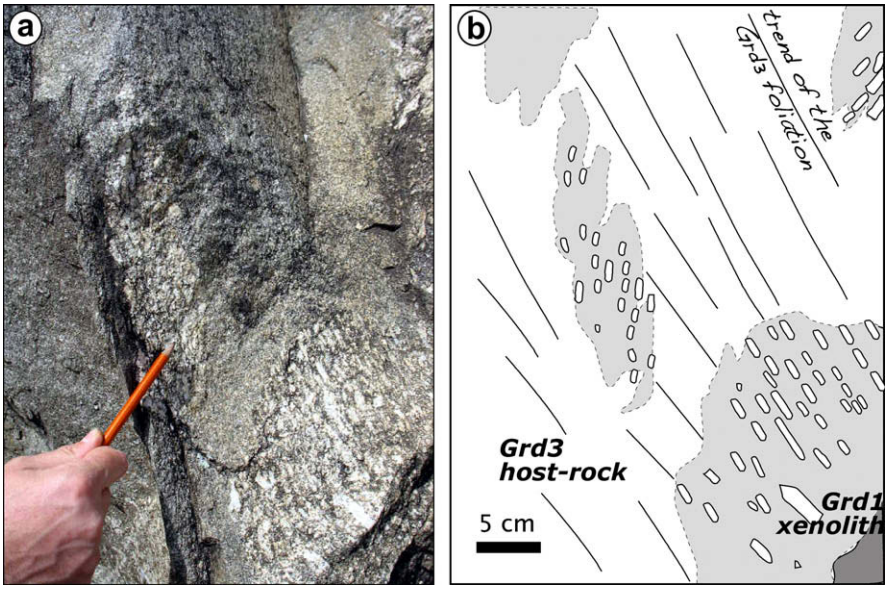

Fig. 7. Relationship between the Grd1 and Grd3 granodiorites. (a) Grd1 granodiorite enclaves in the equigranular Grd3 granodiorite and (b) structural sketch. The Grd3 foliation does not deflect around the enclaves, suggesting that the enclaves were not solid object when they were included in the Grd3 granodiorite. Outcrop location in Fig. 5g,h.

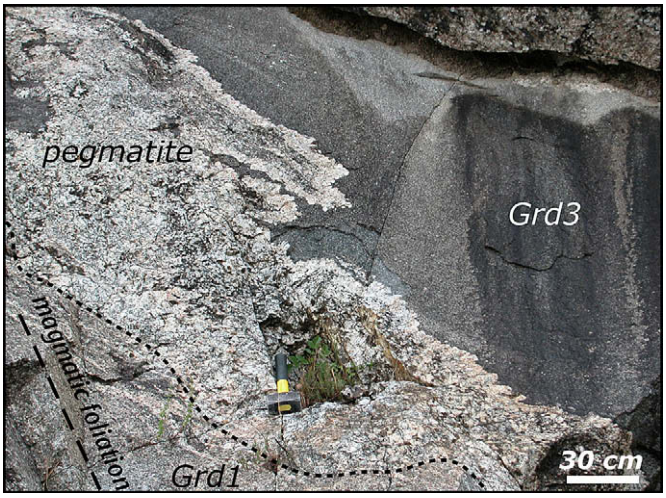

Fig. 8. Relationship between the Grd1 and Grd3 granodiorites. A thick pegmatite layer with chilled margins marks the Grd1/Grd3 boundary, suggesting a local segregation of acidic melts during the Grd3 emplacement into the crystallising Grd1 (compare with Fig. 3c); outcrop location in Fig. 5g,h.

Fig. 10. Pervasive foliation affecting the tonalite and the intruding granite dyke. The margin of the dyke is affected by a shear foliation, interpreted as coeval with the dyke emplacement. Outcrop location in Fig. 5e,f.

Some general considerations can be made on nature and evolution of magmas by examining diagrams in Fig. 4. The AFM plot outlines an arrangement of data points along a typical calc-alkaline trend, except for the mafic rocks (Fig. 4a). The latter show a notable scattering, beyond the boundary dividing the calc-alkaline from the tholeiite suites. The diagram in Fig. 4b allows estimation of an Alkali–Lime index of 58 wt.%, typical of calc-alkaline suites and compatible with late orogenic timing of magma activity (D'Amico et al., 1987).

Harker diagrams (Fig. 4c–f) display nearly linear trends for some oxides (e.g. Fe_2O_{3t} diagram) or a notable dispersion of data points representative of the more mafic rock types (e.g. Al_2O_3, MgO and Sr diagram). This is possibly connected with variable accumulation of pyroxenes and amphibole. Evolution from tonalitic to granodioritic compositions, according to least-squares calculations, can be compatible with crystal fractionation and, chiefly, of plagioclase and amphibole with minor involvement of biotite and ilmenite. The transition from metaluminous to peraluminous compositions, occurring around 60 wt.% in silica content (Fig. 4g), can be justified if amphibole was abundant in the fractionating assemblage (Cawthorn and Brown, 1976). Alternatively, this suggests a significant contamination or mixing with crustal material. In fact, some acidic rocks have values of the A/CNK ratio close or higher than 1.1, reflecting S-type characteristics (White and Chappell, 1988) and a dominant contribution from the continental crust in their genesis (Caggianelli et al., 2003).

In synthesis, despite the different timing of emplacement (see section 4), intrusive rocks involved in the study area share common chemical affinities. Their compositional features fit well in the petrogenetic scenario depicted by Rottura et al. (1990) and Ayuso et al. (1994) for the late Hercynian plutonism in Calabria, on the basis of geochemical and isotopic features. According to these authors, the precursor mantle magmas underplated in a late- to post-collision tectonic setting, undergoing crystal fractionation and contamination with crustal material, acquiring progressively a hybrid nature. The presence of noritic xenoliths in the studied area is in agreement with early orthopyroxene crystallisation favoured by contamination of mantle magmas with crustal material (Campbell, 1985).

In subsequent evolution, heating of the lower crust by the underplated mantle magmas generated anatectic melts that mixed with the contaminated magmas in the route to the final emplacement site, thus producing, together with crystal fractionation, the wide spectrum of the observed compositions.

4. Chronology of magmatic intrusions

Cross-cutting relationships detected along the study section (Fig. 5) led to a chronology of magmatic intrusions, that from old to young is: K-feldspar megacryst-bearing granodiorite carrying mafic enclaves (Grd1) and heterogranular dark granodiorite (Grd2), equigranular granodiorite (Grd3), tonalite, granite. Fabric observations indicate that multiple magma injections occurred when melt

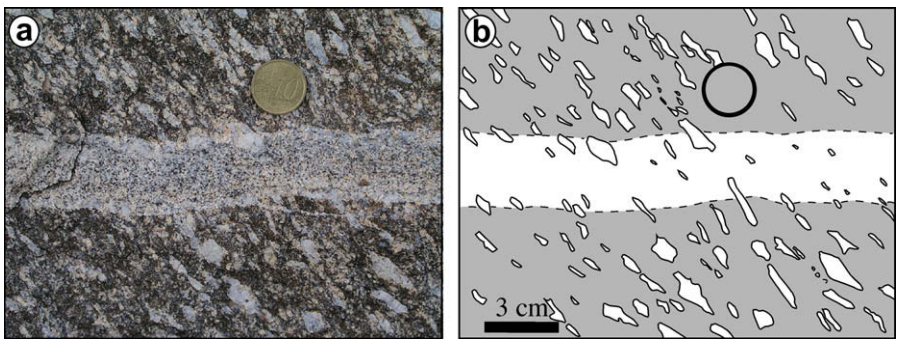

Fig. 9. Grd1/granite veinlet relationship (a) and its structural sketch, based on thin section observation (b). The magmatic foliation cross-cuts the chemical boundary without changing attitude, suggesting its development in melt-present conditions; outcrop location in Fig. 5g,h.

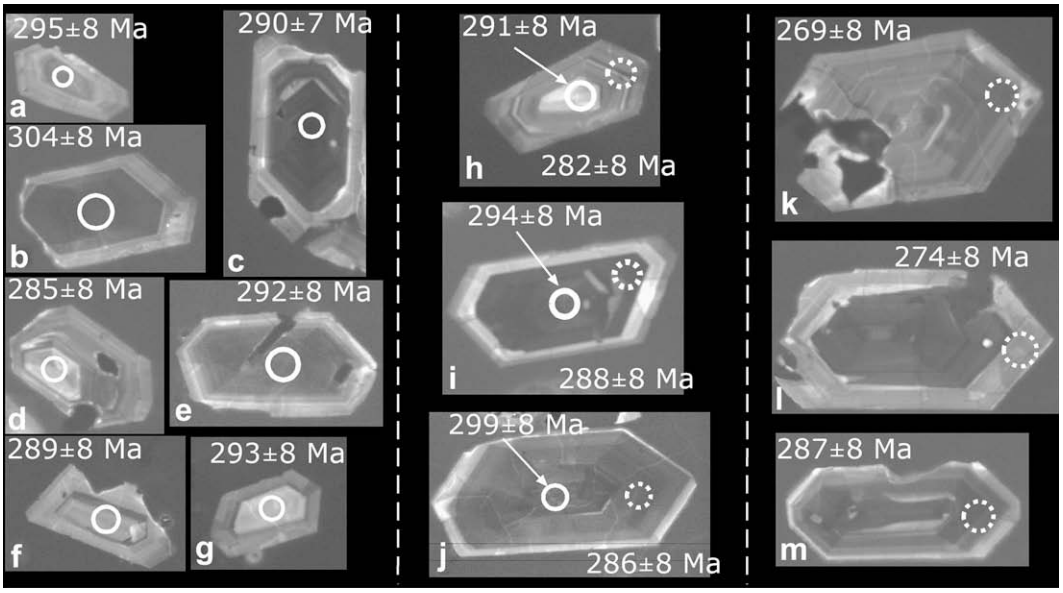

Fig. 11. CL images of analysed zircons from a porphyritic dyke. Circles have a diameter of 25 μm and represent analysed (or ablated) areas. Dashed circles are relative to rims of crystals.

was still present in the magmatic host-rocks. Granodiorites, tonalite and granite are followed by poorly foliated hornblende-gabbro and finally by unfoliated leucogranite, pegmatites and porphyritic dykes. Wall-rocks are intruded by tonalite magmas, with a thickness ranging from few centimetres to 5 m, almost parallel to the NE-dipping basement foliation, over about 500 m perpendicular to strike. All granodiorites, tonalite and granite coexisted as crystal mushes, for periods between 303–302 Ma and 281 ± 8 Ma, as described in Section 5. The reconstruction of the chronology of magmatic intrusions is based on the following field observations.

4.1. Grd1 granodiorite–mafic enclaves relationship

Swarms of dioritic enclaves, cropping out as disrupted and disaggregated dykes (Fig. 3f), show margins that are partly parallel to and partly intersected by the Grd1 magmatic foliation, defined by euhedral (Fig. 6) K-feldspars (more arguments in Section 6.1). Enclaves display variable elongation and their boundaries are from saw-tooth to smooth, in response to viscosity contrast among the involved magmas (Tobisch et al., 1997 and references therein; Paterson et al., 2004). Within the mafic enclaves, patches of Grd1 granodiorite are also observed, suggesting reciprocal mingling relationships. Grd1 granodiorite carries also rare xenoliths of norite (Fig. 3g). Since norite is only rarely observed in the exposed Calabria late Hercynian lower crust, we argue that the occurrence of these xenoliths indicate magma contamination (Campbell, 1985) at deeper crustal levels.

4.2. Grd2–Grd3 granodiorite relationship

The relationship between these two magmatic rocks is shown in Fig. 3c. The equigranular granodiorite (Grd3) is here a dyke injecting the heterogranular dark granodiorite (Grd2) obliquely to its foliation. Consequently, Grd3 is younger than Grd2. The Grd3 cuspate margins are separated from the host-rock by a centimetre-thick pegmatite. Grd3 cusps indicate a minor viscosity of the Grd3

Table 2
LA-ICP-MS analytical results

Zircon	$^{206}Pb/^{238}U$		$^{207}Pb/^{235}U$		$^{207}Pb/^{206}Pb$		$^{208}Pb/^{232}Th$	
	Ratio	1σ (%)	Ratio	1σ (%)	Ratio	1σ (%)	Ratio	1σ (%)
Zr A core	0.047	1.40	0.334	1.91	0.052	1.51	0.015	1.88
Zr B core	0.048	1.38	0.349	1.83	0.052	1.44	0.016	1.87
Zr C core	0.046	1.31	0.325	1.84	0.051	1.49	0.014	1.83
Zr D core	0.045	1.40	0.327	1.90	0.053	1.52	0.014	1.89
Zr E core	0.046	1.47	0.336	1.89	0.053	1.45	0.014	1.88
Zr F core	0.046	1.46	0.329	1.93	0.052	1.50	0.014	1.92
Zr G core	0.046	1.46	0.334	1.99	0.052	1.58	0.014	1.92
Zr H core	0.046	1.38	0.327	1.88	0.051	1.51	0.015	1.88
Zr H rim	0.045	1.39	0.316	1.86	0.051	1.47	0.015	1.87
Zr I core	0.047	1.37	0.332	1.81	0.051	1.41	0.015	1.84
Zr I rim	0.046	1.43	0.329	1.88	0.052	1.45	0.014	1.89
Zr J core	0.048	1.34	0.336	1.80	0.051	1.43	0.016	1.84
Zr J rim	0.045	1.35	0.326	1.81	0.052	1.43	0.014	1.86
Zr K rim	0.043	1.51	0.307	2.00	0.052	1.55	0.013	1.92
Zr L rim	0.043	1.40	0.312	2.00	0.052	1.66	0.014	1.90
Zr M rim	0.046	1.46	0.322	1.88	0.051	1.44	0.014	1.90

Table 3
LA-ICP-MS age results

	$^{206}Pb/^{238}U$		$^{207}Pb/^{235}U$		Concordant age				$^{207}Pb/^{206}Pb$		$^{208}Pb/^{232}Th$	
	Age (Ma)	1σ error	Age (Ma)	1σ error	Age (Ma)	2σ error	MSWD	Prob.	Age (Ma)	1σ error	Age (Ma)	1σ error
Zr A core	295	4	293	6	295	8	0.34	0.56	281	4	292	5
Zr B core	305	4	304	6	304	8	0.04	0.85	298	4	318	6
Zr C core	291	4	286	5	290	7	2.60	0.11	255	4	282	5
Zr D core	285	4	288	5	285	8	0.59	0.44	309	5	285	5
Zr E core	292	4	294	6	292	8	0.60	0.42	312	5	286	5
Zr F core	289	4	289	6	289	8	0.07	0.80	280	4	286	5
Zr G core	293	4	293	6	293	8	0.02	0.97	296	5	285	5
Zr H core	292	4	287	5	291	8	2.30	0.13	251	4	292	5
Zr H rim	283	4	279	5	282	8	2.40	0.12	242	4	293	5
Zr I core	295	4	291	5	294	8	1.90	0.17	259	4	294	5
Zr I rim	288	4	289	5	288	8	0.01	0.93	294	4	284	5
Zr J core	300	4	294	5	299	8	3.00	0.085	251	4	316	6
Zr J rim	286	4	287	5	286	8	0.20	0.65	297	4	283	5
Zr K rim	269	4	272	5	269	8	1.30	0.26	301	5	264	5
Zr L rim	273	4	275	6	274	8	0.31	0.58	287	5	278	5
Zr M rim	288	4	283	5	287	8	3.00	0.09	238	3	276	5

magma with respect to the pegmatite (see also Section 4.3 and Fig. 8). This feature can be explained through two different hypotheses: (i) the Grd3 granodiorite was rich in fluids to such an extent to be less viscous than the pegmatite melt; (ii) the Grd3 injection was channelled along the same path previously followed by the pegmatite, partially crystallised (i.e. with increased viscosity) when the Grd3 dyke emplaced.

4.3. Grd1–Grd3 granodiorite relationship

The equigranular granodiorite (Grd3) contains Grd1 enclaves (Fig. 7), which are generally rounded or show elliptical shape. The Grd3 foliation does not wrap around the enclaves, suggesting that these still contained melt when they were incorporated in the Grd3 magma.

The Grd1–Grd3 structural relationships (Fig. 8) are similar to those already described in Section 4.2: (i) the Grd3 margins are oblique to the host-rock foliation; (ii) a ~70 cm thick pegmatite separates the Grd3 and Grd1 granodiorites; (iii) the cuspate margin indicates first, that both rocks contained melt and second, that viscosity of Grd3 was lower than that of pegmatite; (iv) the boundary between pegmatite and Grd1 is transitional, suggesting that the pegmatite rimming the Grd3 probably represents the interstitial melt expelled from the surrounding Grd1 crystal mush.

Following these lines of evidence, together with the described Grd2–Grd3 relationship (Section 4.2), the Grd3 granodiorite is interpreted as a dyke injecting both the Grd1 and Grd2 granodiorites and, consequently, as being younger.

4.4. Grd1–Grd2 granodiorite relationship

The Grd2 granodiorite crops out in the eastern part of the study section and overlies the Grd1 granodiorite (Fig. 5h,i). The boundary between the two granodiorites is gradual over ~10 m. Going from the Grd1 to the Grd2 granodiorite, gradation is indicated by (i) the progressive size reduction of the aligned euhedral feldspars of Grd1, (ii) the increase in biotite amount and (iii) the change from euhedral to lenticular-shape of feldspars. Foliations in the Grd1 and Grd2 rocks commonly dip ~60° to the NE and are parallel to the lithological boundary between Grd1 and Grd2. These characteristics of the lithological boundary and the common foliation suggest that the Grd1 and Grd2 granodiorites shared the same kinematics starting from melt-present conditions and, therefore, were nearly coeval.

4.5. Tonalite–Grd1 granodiorite relationship

Tonalite intruded the Grd1 and wall-rock (Fig. 5a,b, d,e, f,g). This implies that the tonalite follows the emplacement of the Grd1–Grd2 granodiorites and probably also emplacement of the Grd3. The boundary between tonalite and Grd1 granodiorite is parallel to the Grd1 magmatic foliation (Fig. 5f,g) and dips ~50° to the NE. As indicated in Section 4.7, tonalite and Grd1 are syn-kinematic over a certain period of time.

4.6. Grd1 granodiorite–granite relationship

In the Grd1, the granite is only exposed as cm- to dm-thick dykes. Margins of these dykes can be parallel to the Grd1 magmatic foliation or transect it. In the latter case (Fig. 9), the magmatic foliation cross-cuts the lithological boundary with no deflections. Accordingly, euhedral K-feldspars straddle obliquely the Grd1–granite margin. Such features indicate that foliation developed in melt-present conditions in both host-rock and dyke (Paterson et al., 1989; Vernon, 2000).

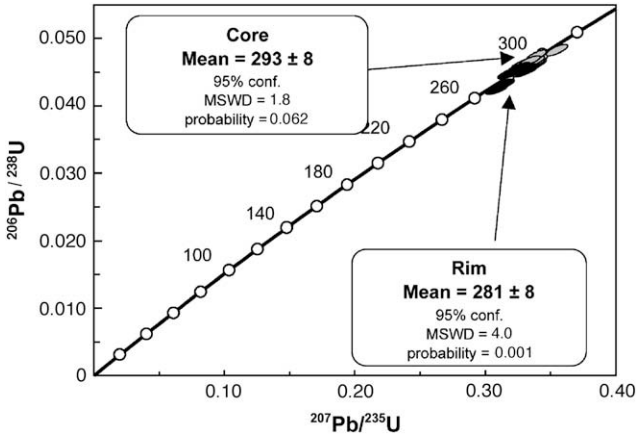

Fig. 12. Concordia diagram showing LA-ICP-MS U/Pb geochronologic data of inner (grey ovals) and outer parts (black ovals) of zircon crystals. The indicated ages derive from weighted averages of the single dates.

4.7. Tonalite–granite relationship

Tonalite is intruded by at least two granite dykes. The larger one, approximately 15 m thick (Fig. 5d,e and e,f), incorporates elongate tonalite enclaves. Their flat faces are parallel to the granite magmatic foliation that, in turn, is parallel to the magmatic to solid-state tonalite foliation. At the outcrop scale, the central parts of the granite dykes are characterised by a strong and pervasive magmatic to solid-state foliation (Fig. 10), parallel to the lithological boundary and to the tonalite foliation. In contrast, close to the dyke margin a planar anisotropy can be locally observed at an angle of ~45° to the lithological boundary. Such anisotropy is interpreted as a shear foliation, coeval with the injection of the acidic magma into the tonalite. All these observations suggest that granite, tonalite and Grd1 granodiorite, coexisted as crystal mush over a certain period of time.

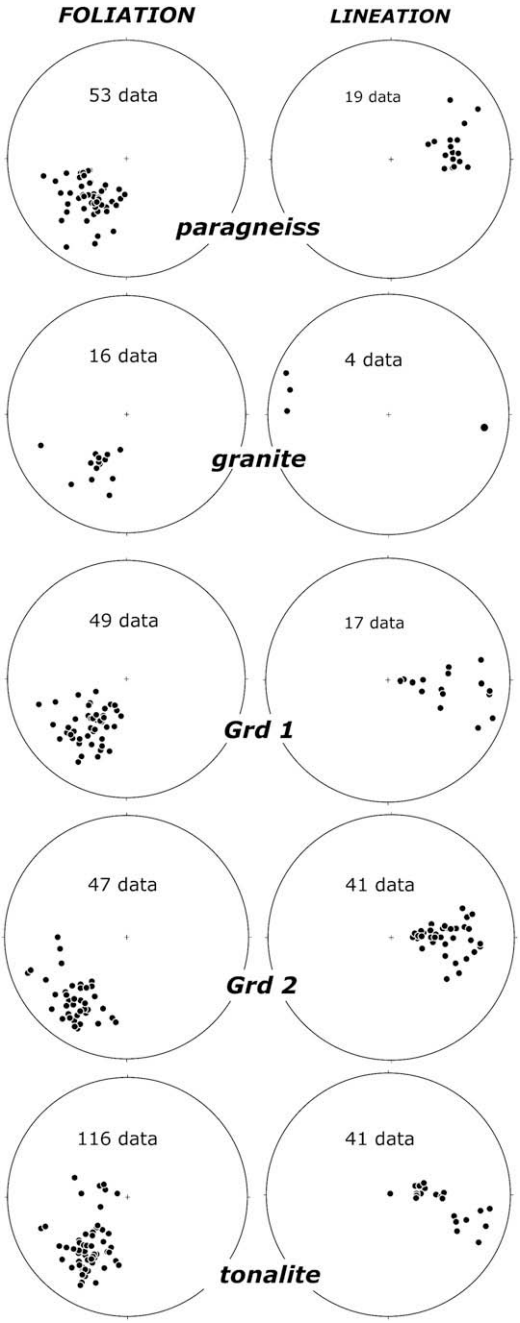

Fig. 13. Orientation diagrams of foliations and mineral lineations from the indicated lithologies. Equiangular projection, lower hemisphere. Data were plotted with Stereonet 6.3.2X by R. Allmendinger.

4.8. Hornblende-gabbro–tonalite–Grd1 granodiorite relationships

Hornblende-gabbro intrudes tonalite and Grd1 granodiorite (Fig. 5c,d and d,e). The contacts of the gabbro to the host-rocks dip

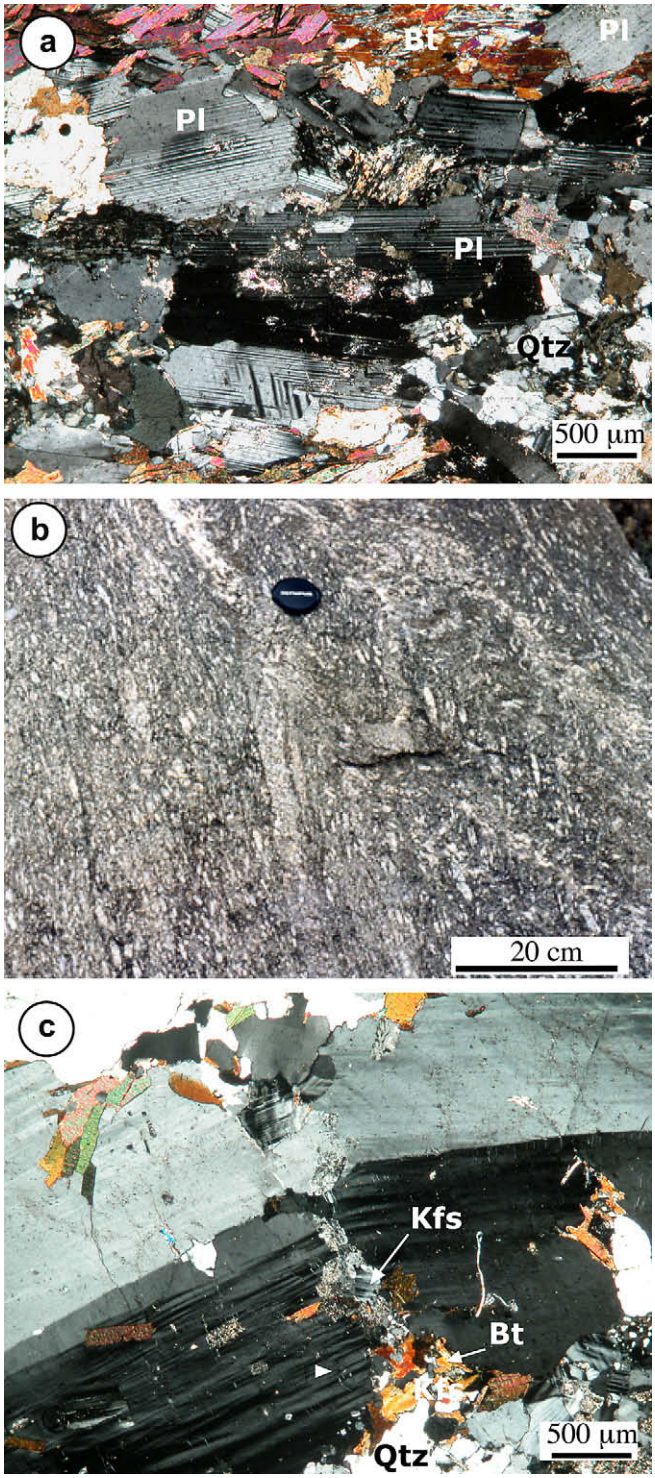

Fig. 14. Micro- and meso-structural features of magmatic deformation. (a) Magmatic foliation in tonalite marked by the alignment of subhedral plagioclase; crossed polars. (b) Magmatic fold in the Grd1 granodiorite, defined by aligned K-feldspar megacrysts; outcrop location in Fig. 5g,h. (c) Magmatic fracture in a K-feldspar crystal: crystallisation of biotite, K-feldspar and quartz in the magmatic vein. Crossed polars.

~70° to the NE but are not clearly exposed. In contrast to tonalite and Grd1, the hornblende-gabbro is weakly foliated and the orientation of foliation varies from W-dip over sub-horizontal to E-dip. It remains open if the wall-rocks were solid or crystal-mush when the gabbro intruded but the completely different orientation of the magmatic foliation in the gabbro argues for a kinematic tectonic framework different from the one affecting earlier granite, tonalite and granodiorites. Alternatively, it may be supposed that the gabbroic magma crystallised faster than hosting granodiorite and tonalite magmas. After full crystallisation, the mineral composition of the hornblende-gabbro made it a strong and rigid body, located within the granitoid magmas. In this view, the weak foliation of the hornblende-gabbro should reflect the magma kinematics (near strain field) and not the kinematics imposed by the regional tectonic context (far strain field).

4.9. Leucogranite, pegmatite, porphyritic rocks

Basement rocks, tonalite, Grd1 and Grd2 are intruded by non-foliated leucogranite, non-foliated pegmatite, felsic and mafic porphyritic rocks. All these rocks are interpreted as post-kinematic with respect to the magmatic foliation of their host-rocks (Fig. 5).

5. Age of post-tectonic intrusions

Dated post-tectonic intrusions are represented by leucogranites and pegmatites. Leucogranites cropping out in the Sila Massif near the Cecita Lake (Fig. 1) provided a Rb/Sr isochron age of 284 ± 14 Ma (Caggianelli et al., 2000). An undeformed pegmatite from the Mesoraca area in clear cross-cutting relationships with heterogranular dark granodiorites (Grd 2) gave a Rb/Sr muscovite whole rock age of 265 ± 3 Ma (Festa et al., 2001; Fig. 1). The gap between these two ages in large amount can be attributed to the adoption of diverse dating methods that imply different closing temperatures. In fact, reasonable Rb/Sr closing temperatures for whole rock isochron and muscovite methods are around 700 °C (e.g. Hollister, 1982) and 500 °C (Wagner et al., 1977), respectively. In addition, recent data are available from a felsic porphyritic dyke that was dated by U/Pb method, using LA-ICP-MS (see Appendix A). The dyke is exposed close to the Arvo Lake (Fig. 1), ~40 km north of the study area (Langone, 2007). On cathodoluminescence images zircons are euhedral and prismatic (mean aspect ratio of 2.04) with concentric oscillatory zoning from core to rims, indicative of igneous origin (Fig. 11).

Generally, crystal luminescence is faint in cores and bright in rims (Fig. 11). Only few crystals show inverse luminescence intensities (Fig. 11D,G,H). In some cases we observed zircons having a core with an irregular outline (Fig. 11M) surrounded by a rim with oscillatory zoning. These probably represent former xenocrysts partially resorbed and then overgrown by shells in equilibrium with the evolving acidic magma. Analyses have been performed using a laser spot size of 25 μm and isotopic compositions have been collected from different portions of selected crystals with contrasting luminescence intensities (Fig. 11). Isotopic ratios and a summary of concordant LA-ICP-MS ages are reported in Tables 2 and 3, respectively, whereas a concordia diagram is shown in Fig. 12. As expected, ages relative to inner portions of crystals are older than those obtained from the outer parts, with an average of 293 ± 8 and 281 ± 8 Ma, respectively. Undisturbed internal oscillatory zoning of zircons coupled with geochronologic data becoming progressively younger towards the outer crystals parts, is compatible with continuous magmatic growth. The older ages obtained in the inner zones, easily identified on the basis of the contrasting luminescent properties, could be linked to the early stage of crystallisation in a deeper magma chamber whereas the younger ages could be linked to the final stage of crystallisation at the shallow emplacement level of the porphyritic dykes.

6. Structures of magmatic intrusions and wall-rocks

In this section we describe meso- to micro-structures of all different rocks in more detail in order to demonstrate that all magmatic rocks as well as the basement were affected by a common kinematic framework during crystallisation of the magmas and subsequent regional cooling from high- to low-T conditions. Our description starts with the analysis of the common magmatic foliation and lineation and proceeds with the examination of the structures produced from high-T to progressively lower-T conditions in both magmatic and basement rocks. The transition from magmatic to totally solid state is also discussed.

6.1. Magmatic structures

In the magmatic rocks of the study section and surroundings a pervasive planar anisotropy with alignment of euhedral minerals (mostly amphibole, biotite and feldspars), and mafic enclaves (Fig. 3b,f) is present. It strikes about 140° with a dip of 50–60° to the NE, roughly parallel to the host-rock foliation (Fig. 13) and to the contact with the metamorphic basement (Fig. 5a,b). The bulk of euhedral minerals, observed on the XZ plane, i.e., parallel to the mineral lineation, do not show pressure shadows, suggesting that they were aligned mostly under melt-present conditions (Vernon, 2000; Vernon et al., 2004).

Considering that (i) the observations are structurally located close to the border of the basement, (ii) the foliation in granitoids is almost parallel to this border and parallel to sub-parallel to the internal boundaries of the magmatic bodies (Fig. 5), and (iii) in general the magmatic intrusions of the Sila represent large-scale

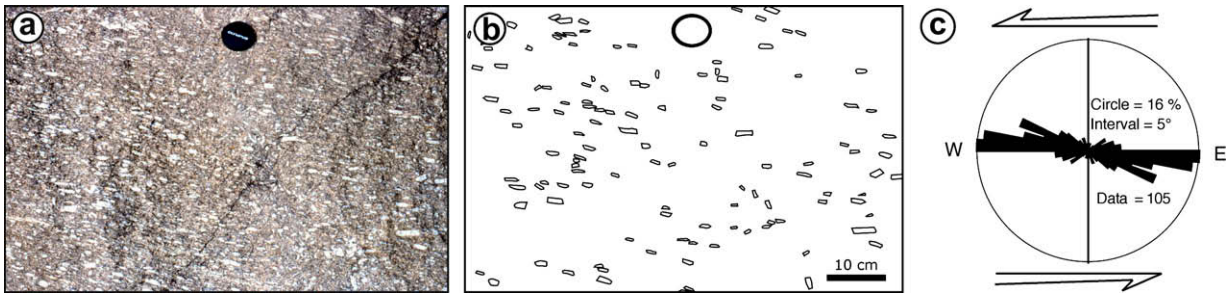

Fig. 15. Distribution of the euhedral to subhedral K-feldspar megacrysts long axes measured in the XZ plane, parallel to the mineral lineation; only crystals with aspect ratios larger than 2 and long axes larger than 1.2 cm were taken into account. Photograph (a) and sketch (b) of the analysed outcrop within the Grd1 granodiorite. (c) Orientation rose diagram of the K-feldspar long axes. The length of branches is indicated in percentage and their width is 5°. Considering the plane of maximum orientation as the magmatic shear plane, the asymmetry of K-feldspar distribution indicates the magmatic shear sense. Outcrop location in Fig. 5g,h.

sills (Caggianelli and Prosser, 2001), the plane of mineral alignment is interpreted as magmatic flow plane, i.e., as magmatic foliation.

In the tonalite, the magmatic foliation is expressed by a pervasive planar anisotropy marked by alignments of euhedral or subhedral biotite and plagioclase (Fig. 14a). The latter sometimes is zoned and poikilitic, enclosing euhedral biotite flakes, typically 0.3 μm across.

In the granite, the occurrence of a magmatic planar anisotropy is suggested by the preferred orientation of subhedral K-feldspars and of ~20 μm long lenses made up of quartz and biotite. Conversely, in the hornblende-gabbro magmatic foliation appears to be weak in the field although, in thin section, it is well characterised by alignment of large subhedral and zoned plagioclase and amphibole (mostly cummingtonite).

However, the most striking mineral alignment is related to the K-feldspar megacrysts from the Grd1 (Fig. 3a). Only in this strongly foliated rock a magmatic mineral lineation is well developed and represented by the alignment of long axes of the centimetric tabular K-feldspar megacrysts. This lineation dips of about 20° towards the E, on average (Fig. 13). Differently, the matrix (of millimetre size) does not show any evident linear anisotropy. Grd1 fabrics are also characterised by folds (Fig 14b). At the microscopic scale, rare fractures in coarse K-feldspar are sealed with quartz, feldspars and biotite (Fig. 14c).

Elongate enclaves, folds and fractures are interpreted as melt-present deformation features (Bouchez et al., 1992; Tobisch et al., 1997; Paterson et al., 1998) of the K-feldspar megacrystals-bearing granodiorite.

Locally, in the K-feldspar-bearing granodiorite, tiling of feldspar phenocrysts suggests that shearing was active during magmatic flow. In addition, at one locality, the distribution of K-feldspar long axes is asymmetric (Fig. 15) with respect to the magmatic foliation. From this asymmetry, together with the local occurrence of tiling structures, a top-to-the-west sense of shear during magmatic flow can be inferred, following criteria adopted in other studies (Blumenfeld and Bouchez, 1988; Ildefonse and Fernandez, 1988; Vernon, 2000; Spanner and Kruhl, 2002).

6.2. Structures transitional from magmatic to solid-state

Here we describe structures that formed during cooling and crystallisation of magmas in a regional stress field that also affected the wall-rocks.

In the foliated granitoids, structures testifying a continuum from HT to LT deformation conditions have been recognised. Deformation temperatures are provided by the commonly observed chessboard subgrain pattern (Fig. 16a) of quartz in all the granodiorites. This type of prism- and basis-parallel subgrain-boundary

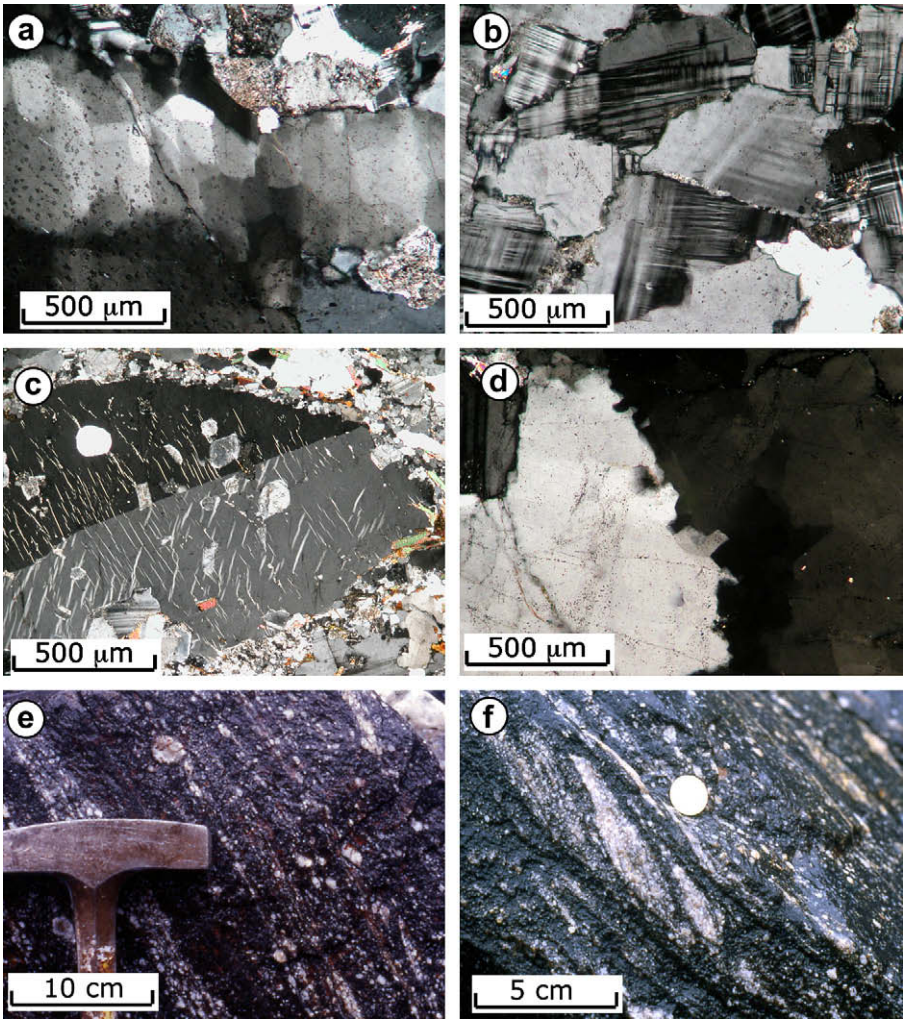

Fig. 16. Meso- and micro-structures indicating the transition from magmatic to solid-state deformation. From a to d, in order of decreasing temperatures: (a) chessboard subgrain pattern in quartz, crossed polars; (b) recrystallisation of K-feldspars; (c) myrmekite structure with perthitic flames; (d) grain-boundary migration in quartz; (e) quartz ribbons and rounded feldspars; outcrop location in Fig. 5h,i; (f) S/C structures indicating a top-to-the-west sense of shear; outcrop location in Fig. 5h,i.

pattern solely develops in the stability field of high-quartz (Kruhl, 1996). Since the boundary between low- and high-quartz is at ~700 °C at ~5 kbar—the approximate pressure of intrusion for the sheared granitoids (Caggianelli et al., 1997)—a minimum temperature of deformation of ~700 °C is indicated.

Universal-stage measurements of quartz *c*-axis have been carried out on samples from migmatitic paragneiss (Fig. 17b), foliated tonalites (Fig. 17a,c,d) and granodiorites (17e–h). The crystallographic preferred orientations (CPOs) show mostly a monoclinic symmetry. Three different point maxima have been recognised: (i) a pair of point maxima with angles of ~100–130° across strain-Z (Fig. 17a–h); (ii) point maxima close to strain-Z (Fig. 17b–d,g,h); (iii) point maxima close to strain Y (Fig. 17a–e,g). These point maxima are generally referred to the activation of prism [c], basal <a> and prism <a> slip systems, respectively (e.g., Garbutt and Teyssier, 1991, and references therein).

Again, these opening angles of quartz *c*-axes cross girdles of type (i) indicate deformation temperatures of about 700 °C (Kruhl, 1998), in agreement with the temperatures inferred from quartz chessboard subgrain pattern.

A top-to-the-west shear sense both in migmatitic paragneiss and in syn-tectonic plutonic rocks (Fig. 17a–c,e,f) can be deduced from different densities of point maxima related to prism [c] glide system in most samples (e.g. Schmid and Casey, 1986). This shear sense is coherent with outcrop- and micro-scale kinematic indicators.

In some samples (i.e. Fig. 17a and c) orientation of point maxima located near strain-Z is coherent with top-to-the-west shear sense along the basal <a> slip system, as already deduced from maxima related to prism [c] slip system. In other samples (Fig. 17b,d,g), strong point maxima located close to strain-Z apparently suggest a contrasting shear sense. This apparent contradiction may be explained by the fact that, starting from the initial high temperature maxima, the quartz *c*-axis would necessarily rotate toward strain-Z, due to dominant activity of basal <a> glide during low temperature coaxial flattening (Garbutt and Teyssier, 1991; Duguet and Faure, 2004).

Evidence of prismatic <a> slip, indicated by *c*-axis maxima subparallel to strain Y (Fig. 17a–e,g), is consistent with deformation at intermediate to high temperatures (Stipp et al., 2002).

Summing up, *c*-axis CPOs are coherent with solid-state deformation at high to low temperature conditions. *c*-axis patterns can be explained by the dominance of prism <a> glide at high temperatures or by transition from dominant prism <a> to prism <a> to basal <a> slip systems at decreasing temperatures.

6.3. Structures at medium- to low-temperature solid-state conditions

Deformation under decreasing temperatures is pointed out by coarse-grained (Fig. 16b) as well as fine-grained recrystallisation of feldspars, widespread occurrence of myrmekite (Fig. 16c), and grain-boundary migration recrystallisation in the quartz ribbons (Fig. 16d), especially in the heterogranular granodiorite (Grd2). In this rock the solid-state fabric is defined by strong alignment of biotite plates and the flat faces of lenticular feldspars and elongate quartz aggregates (Fig. 16e). Locally, the Grd2 displays S/C fabrics (Berthé et al., 1979), pointed out by biotite films and thin quartz-feldspar layers (Fig. 16f). Mineral lineation (about 85/25) is mainly outlined by quartz and feldspar long axes. S/C fabrics and delta- and sigma-type feldspar porphyroclasts confirm a top-to-the-west sense of shear.

6.4. Structures in the wall-rocks

In the migmatitic paragneisses the main foliation is generally oriented 45/40 (Fig. 13). This is defined by the compositional layering of well-aligned fine-grained mica, sillimanite and cordierite, alternating with quartz-feldspar-rich bands. Hinges of intrafolial folds are rare, probably due to the intense transposition during deformation.

The mineral lineation, oriented 85/25 on average (Fig. 13), is defined by long axes of sillimanite, cordierite, biotite, and quartz

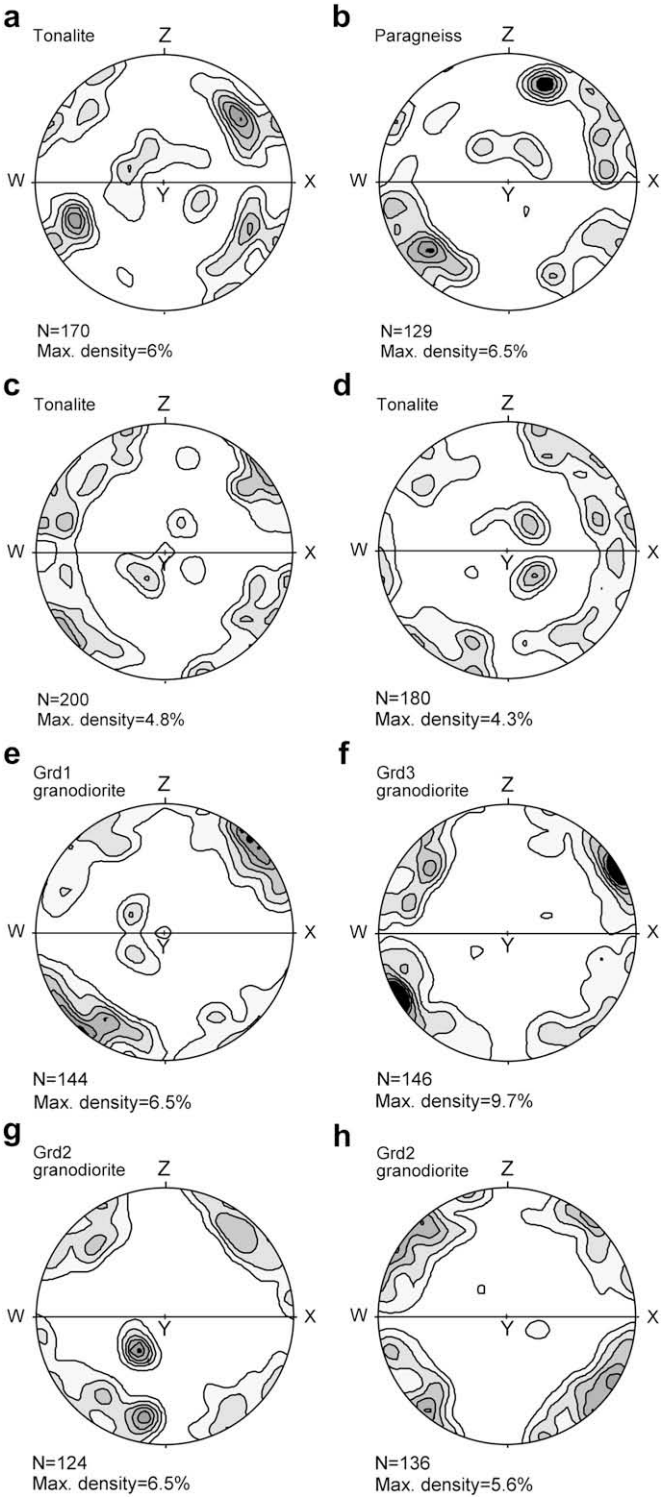

Fig. 17. Quartz *c*-axis fabrics (equal area projection, lower hemisphere) from samples of tonalite, paragneiss and granodiorites, obtained by universal stage. X is stretching lineation, Z is normal to foliation and stretching lineation and Y is perpendicular to X and Z reference frame. Data show mostly a monoclinic symmetry. Contours at 1, 2, 3, 4, 5 and 6% for 1% area. Location of samples: *a* and *b* in Fig. 5a,b; *c*, in Fig.5b,c; *d* in Fig. 5e,f; *e* and *f* in Fig. 5g,h; *g* and *h* in Fig. 5h,i.

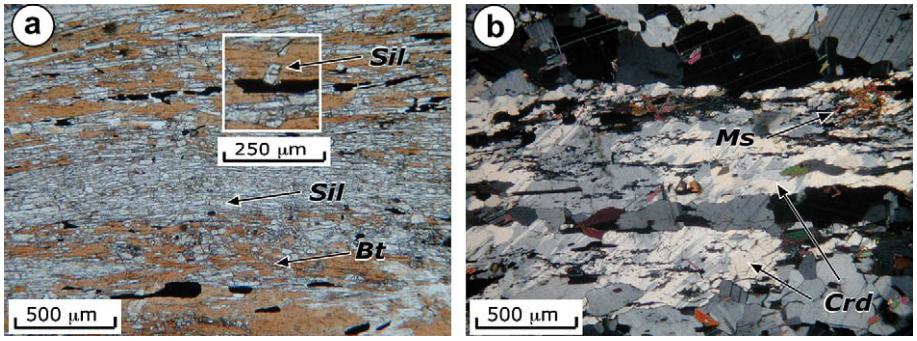

Fig. 18. Fabric anisotropy within the migmatitic paragneiss refers to oriented sillimanite (Sil) needles and biotite (Bt) plates (plane polarised light). The white square highlights a post-kinematic sillimanite at a greater magnification. (b) Cordierite (Crd) and muscovite (Ms) layers intervening within layers rich in quartz and plagioclase (crossed polars).

grains. This peak-metamorphic mineral assemblage (Graessner and Schenk, 2001) indicates that foliation as well as lineation was formed during maximum temperature conditions of 740–770 °C. A widespread crystallisation of post-kinematic white mica and fibrous sillimanite can be observed (Fig. 18a,b). Rims of garnet porphyroblasts are replaced by cordierite, indicating decompression, as well as biotite–sillimanite aggregates, indicating cooling (Graessner and Schenk, 2001). The occurrence of cordierite, biotite and sillimanite in garnet pressure shadows points to continuous deformation during decreasing pressure and temperature. σ-type garnet porphyroclasts, mica-fishes and c-axis analyses (Fig. 17b) indicate top-to-the-west sense of shear.

7. Discussion

The relationships among the different magmatic rocks are sketched in Fig. 19. The chronology of emplacement is based on field relationships, by which the Grd1 and the Grd2 are considered the first magmatic bodies to be emplaced. Then, the Grd3 injected both previous granodiorites still in melt-present conditions. The sequence of injections continued with the tonalite magma and afterwards with the granite dykes. The emplacement of the hornblende-gabbro is interpreted as a late magmatic episode with respect to the deformation history in the granodiorites, tonalites and granites. The injection sequence ended with the emplacement of non-foliated post-kinematic leucogranite, pegmatite and porphyritic dykes.

Meso- and micro-structural observations suggest that shearing of wall-rocks and magmatic intrusions occurred under the same kinematic conditions during injection of Grd1, Grd2, Grd3, tonalite and granite magmas and during their subsequent cooling. The period of deformation can be encompassed between the age of emplacement of the syn-kinematic granitoids (granodiorites, tonalite and granite) and of the undeformed leucogranite, pegmatites and porphyritic dykes.

Age of emplacement of granodiorites, tonalite and granite is regionally well constrained by U/Pb datings at 304–300 Ma; within this time range, the dates near the study section are also encompassed (Graessner et al., 2000). Shearing of the magmas therefore is considered active during emplacement.

Thus, since leucogranite, pegmatites and porphyritic dykes intruded older foliated magmatic and wall-rocks throughout the whole Sila Massif (Ayuso et al., 1994), we reasonably assume that the age of 281 ± 8 Ma from the porphyritic dyke located close to the Arvo Lake (Fig. 1), could at least represent a minimum age for the end of shear deformation. Following this view, injection and shear strain history took place over a period of about 20 Ma although a shorter time range cannot be ruled out.

Concerning the tectonic context in which deformation and emplacement developed, the following considerations can be argued. The late-Hercynian Calabrian crust is palaeogeographically related to the French Massif Central and Sardinia Massif (Matte, 1986, 2001; Stampfli and Borel, 2002; Von Raumer et al., 2002). Petrologic, structural and kinematic data indicate that collision occurred around 350–320 Ma with pressure of 2 GPa at least in Sardinia (Giacomini et al., 2005) or of about 3 GPa in the French Massif Central (Lardeaux et al., 2001). In Sardinia and French Massif Central, ages around 300–310 Ma mark the turning point from contraction to post-collisional extension, favouring the emplacement of syn- to post-tectonic granitoids and the achievement of the metamorphic peak conditions. Then isothermal exhumation and isobaric cooling followed (Burg et al., 1994; Carmignani et al., 1994; Faure, 1995; Ledru et al., 2001; Di Vincenzo et al., 2004, among many others).

Also the late-Hercynian Calabria evolution is typified by the coexistence between magmatism and peak metamorphic conditions at ~300 Ma, followed by isothermal decompression and isobaric cooling. Peak pressure in Calabria is estimated at about 4–6 kbar, in the Sila Massif (Graessner et al., 2000; Graessner and Schenk, 2001) or at about 7.5–8 kbar, in the Serre Massif (Schenk, 1989; Acquafredda et al., 2006). Schenk (1984) and Graessner and Schenk (2001) suggested that emplacement of granitoids and the Calabria peak metamorphic conditions can be developed during contractional tectonics. According to these authors, compression developed in an Andean-type geodynamic context, determining

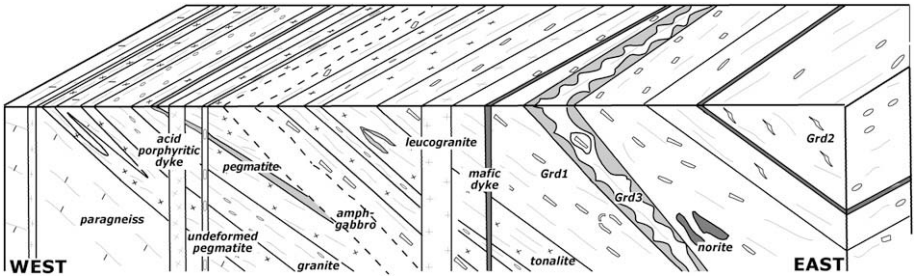

Fig. 19. Block diagram, not to scale, summarising the relationship among granitoids and between wall-rocks and granitoids, as reconstructed from the geological profile shown in Fig. 5.

crustal doubling, heating, partial melting of the overridden plate and high geothermal gradient in the upper crust ($\approx$60 °C/km). Then, erosion was responsible for the isothermal exhumation. This implies that the thickening of the crust took place at about 300 Ma, almost 30–50 Ma later than the Hercynian collision in Sardinia and French Massif Central. However, the magma intrusion would post-date the age of the Palaeozoic phyllite metamorphism in the Sila massif (dated at about 330 Ma: Acquafredda et al., 1991, 1992).

Alternatively, as also indicated by Graessner and Schenk (2001), a post-collisional extensional tectonics (Caggianelli and Prosser, 2001) can be considered. In this tectonic context, also the low- to medium-pressure metamorphism characterising the Calabrian late-Hercynian mid-crust could be easily framed.

Structural and kinematic data collected in the study area do not help to constrain the geodynamic setting, in which shearing and injection occurred; however, the HT conditions in which deformation developed and the similarities with the evolutions of Sardinia and Central Massif suggest extensional tectonics during magma emplacement. Furthermore, the occurrence of norite enclaves in the Grd1 rocks and the broad tendency of the syn-tectonic injections towards mafic compositions, account for a progressive involvement of the lithospheric mantle in the melting process, as is typical during lithospheric thinning (e.g., Wilson, 1993). In this framework, magma underplating would provide an additional source of heating, favouring high geothermal gradient and crustal magma generation.

8. Concluding remarks

Syn-tectonic and post-tectonic magmatic rocks have been recognised in a mid-crustal section. Field data suggest that multiple injections of magmas occurred in crystallising granitoids while shear strain was ongoing. The broad tendency toward a basic composition of magmas suggests a progressive involvement of the mantle in the melting process.

High-temperature deformation affected both crystallising magmas and wall-rocks. Meso- and micro-structural data in the study area document continuous progression of deformation under decreasing temperatures, within the same kinematic framework.

The period of time over which magma injection and shear strain coexisted is enclosed between the emplacement of the syn-kinematic granitoids (304–300 Ma) and emplacement of undeformed porphyritic dyke (281 $\pm$ 8 Ma). Therefore shear strain developed over a period of $\sim$20 Ma as a maximum.

A significant extensional component could provide a tectonic evolution similar to the one characterising other sectors of the southern European Hercynian belt, although more data from other selected areas in Calabria are still necessary to better constrain the geodynamic setting in which shearing and magma injection took place.

Acknowledgements

Financial support from the Italian–German VIGONI program is acknowledged. We are grateful to Paolo Conti and Carlos Fernández whose comments and suggestions helped us to improve the original manuscript.

Appendix A. Geochronologic method

Samples were completely crushed and zircons were separated using conventional heavy liquid and magnetic techniques. Crystals were selected by handpicking under a binocular microscope, mounted in epoxy resin and polished down to expose the major surface of crystal. The selection of zircons for isotope analyses was done on the basis of cathodoluminescence (CL) images acquired with a SEM at the Department of Earth Science in Siena (acceleration voltage 20–25 kV). Geochronologic data were performed using a LA-ICP-MS system coupling a 266 nm Nd:YaG laser probe with a double focusing magnetic-sector mass spectrometer (Tiepolo et al., 2003) at the CNR-IGG of Pavia.

References

Acquafredda, P., Barbieri, M., Lorenzoni, S., Trudu, C., Zanettin Lorenzoni, E., 1991. The age of volcanism and metamorphism of the Bocchigliero Paleozoic sequence (Sila – Southern Italy). Rendiconti Scienze Fisiche e Naturali Accademia dei Lincei 9 (2), 145–156.

Acquafredda, P., Barbieri, M., Lorenzoni, S., Trudu, C., Zanettin Lorenzoni, E., 1992. Metamorphism of the Mandatoriccio Unit in the context of the Hercynian and pre-Hercynian evolution of the Calabrian-Peloritan Arc (southern Italy). Rendiconti Scienze Fisiche e Naturali Accademia dei Lincei 9 (3), 151–161.

Acquafredda, P., Fornelli, A., Paglionico, A., Piccarreta, G., 2006. Petrological evidence for crustal thickening and extension in the Serre granulite terrane (Calabria, southern Italy). Geological Magazine 143, 145–163.

Amodio-Morelli, L., Bonardi, G., Colonna, V., Dietrich, D., Giunta, G., Ippolito, F., Liguori, V., Lorenzoni, S., Paglionico, A., Perrone, V., Piccarreta, G., Russo, M., Scandone, P., Zanettin Lorenzoni, E., Zuppetta, A., 1976. L'Arco Calabro-Peloritano nell'Orogene Appenninico-Magrabide. Memorie della Società Geologica Italiana 17, 1–60.

Atzori, P., Ferla, P., Paglionico, A., Piccarreta, G., Rottura, A., 1984. Remnants of the Hercynian orogen along the "Calabria Peloritan Arc", southern Italy: a review. Journal of the Geological Society of London 141, 137–145.

Ayuso, R.A., Messina, A., De Vivo, B., Russo, S., Woodruff, L.G., Sutter, J.F., Belkin, H.E., 1994. Geochemistry and argon thermochronology of the Variscan Sila Batholith, southern Italy: source rocks and magma evolution. Contributions to Mineralogy and Petrology 117, 87–109.

Berthé, D., Choukroune, P., Jegouzo, P., 1979. Orthogneiss, mylonite and non coaxial deformation of granites: the example of the South Armorican Shear Zone. Journal of Structural Geology 1, 31–42.

Blumenfeld, P., Bouchez, J.L., 1988. Shear criteria in granite and migmatite deformed in the magmatic and solid states. Journal of Structural Geology 10, 361–372.

Bonardi, G., Cavazza, W., Perrone, V., Rossi, S., 2001. Calabria-Peloritani terrane and northern Ionian Sea. In: Vai, G.B., Martini, I.P. (Eds.), Anatomy of an Orogen: The Apennines and Adjacent Mediterranean Basins. Kluwer, Dordrecht, pp. 287–306.

Borsi, S., Dubois, R., 1968. Donnés geochronologiques sur l'histoire hercynienne, et alpine de la Calabre Centrale. Compte Rendu de la Académie des Sciences 266, 72–75.

Bouchez, J.L., Delas, C., Gleizes, G., Nedelec, A., Cuney, M., 1992. Submagmatic microfractures in granites. Geology 20, 35–38.

Brown, G.C., 1982. Calc-alkaline intrusive rocks: their diversity, evolution, and relation to volcanic arcs. In: Thorpe, R.S. (Ed.), Andesites. John Wiley, London, pp. 437–461.

Burg, J.P., Van der Driessche, J., Brun, J.P., 1994. Syn to post-thickening extension in the Variscan belt of western Europe: modes and structural consequences. Geologie de la France 3, 33–51.

Caggianelli, A., Prosser, G., 2001. An exposed cross-section of the late Hercynian and intermediate continental crust in the Sila nappe (Calabria, southern Italy). Periodico di Mineralogia 70, 277–301.

Caggianelli, A., Prosser, G., Di Battista, P., 1997. Textural features and fabric analysis of granitoids emplaced at different depths: the example of the Hercynian tonalites and granodiorites from Calabria. Mineralogica et Petrographica Acta 40, 11–26.

Caggianelli, A., Prosser, G., Del Moro, A., 2000. Cooling and exhumation history of deep seated and shallow level, late Hercynian granitoids from Calabria. Geological Journal 35, 33–42.

Caggianelli, A., Del Moro, A., Di Battista, P., Prosser, G., Rottura, A., 2003. Leucogranite genesis connected with low-pressure high-temperature metamorphism in the Sila basement (Calabria, Italy). Schweizerische Mineralogische Petrographische Mitteilungen 83, 301–316.

Campbell, I.H., 1985. The difference between oceanic and continental tholeiites: a fluid dynamic explanation. Contributions to Mineralogy and Petrology 91, 37–43.

Carmignani, L., Carosi, R., Di Pisa, A., Gattiglio, M., Musumeci, G., Oggiano, G., Pertusati, P.C., 1994. The Hercynian chain in Sardinia (Italy). Geodinamica Acta 7, 31–47.

Cawthorn, R.G., Brown, P.A., 1976. A model for the formation and crystallization of corundum-normative calc-alkaline magmas through amphibole fractionation. Journal of Geology 84, 467–476.

D'Amico, C., Innocenti, F., Sassi, F.P., 1987. Magmatismo e Metamorfismo. UTET, Torino.

D'Lemos, R.S., Brown, M., Strachan, R.A., 1992. Granite, magma generation, ascent and emplacement within a transpressional orogen. Journal of the Geological Society of London 149, 487–490.

Dewey, J.F., Helman, M.L., Turco, E., Hutton, D.W.H., Knott, S.D., 1989. Kinematics of the western Mediterranean. In: Coward, M.P., Dietrich, D. (Eds.), Alpine Tectonics. Geological Society of London, Special Publication 45, pp. 265–283.

Di Vincenzo, G., Carosi, R., Palmeri, R., 2004. The relationship between tectono-metamorphic evolution and argon isotope records in white mica: constraints

from in situ $^{40}Ar/^{39}Ar$ laser analysis of the Variscan Basement of Sardinia. Journal of Petrology 45, 1013–1043.
Dubois, R., 1976. La suture calabro-apenninique cretacee-eocene et l'ouverture Tyrrhenienne neogene: etude petrographique et structurale de la Calabre centrale. Ph.D. Thesis, Univ. P. et M. Curie, Paris.
Duguet, M., Faure, M., 2004. Granitoid emplacement during a thrusting event: structural analysis, microstructure and quartz *c*-axis patterns. An example from Hercynian plutons in the French massif central. Journal of Structural Geology 26, 927–945.
Faure, M., 1995. Late orogenic carboniferous extensions in Variscan French Massif Central. Tectonics 14, 132–153.
Fernandez, C., Castro, A., De La Rosa, J.D., Moreno-Ventas, I., 1997. Rheological aspects of magma transport inferred from rock structures. In: Bouchez, J.L., Hutton, D.H.W., Stephens, W.E. (Eds.), Granite: From Segregation of Melt to Emplacement Fabrics. Kluwer, Dordrecht, pp. 75–91.
Festa, V., Caggianelli, A., Liotta, D., Prosser, G., Del Moro, A., 2001. Structural and petrological features of a ductile shear zone in late-Hercynian granitoids (Sila Massif, Calabria). Geoacta 1, 165–176.
Festa, V., Di Battista, P., Caggianelli, A., Liotta, D., 2003. Exhumation and tilting of the late Hercynian continental crust in the Serre Massif (southern Calabria, Italy). Bollettino della Società Geologica Italiana 2, 79–88.
Festa, V., Caggianelli, A., Kruhl, J.H., Liotta, D., Prosser, G., Guegen, E., Paglionico, A., 2006. Late Hercynian shearing during crystallization of granitoid magmas (Sila Massif, southern Italy): regional implications. Geodinamica Acta 19 (3/4), 185–195.
Garbutt, J.M., Teyssier, C., 1991. Prism <a> slip in the quartzites of the Oakhurst Mylonite belt, California. Journal of Structural Geology 13, 657–666.
Giacomini, F., Bomparola, R.M., Ghezzo, C., 2005. Petrology and geocrhronology of metabasites with eclogite facies relics from NE Sardinia: constraints for the Palaeozoic evolution of Southern Europe. Lithos 82, 221–248.
Graessner, T., Schenk, V., 2001. An exposed Hercynian deep crustal section in the Sila Massif of northern Calabria: mineral chemistry, petrology and a P–T path of granulite-facies metapelitic migmatites and metabasites. Journal of Petrology 42, 931–961.
Graessner, T., Schenk, V., Bröcker, M., Mezger, K., 2000. Geochronological constraints on the timing of granitoid magmatism, metamorphism and post-metamorphic cooling in the Hercynian crustal cross-section of Calabria. Journal of Metamorphic Geology 18, 409–421.
Gueguen, E., Doglioni, C., Fernandez, M., 1998. On the post-25 Ma geodynamic evolution of the western Mediterranean. Tectonophysics 298, 259–269.
Hollister, L.S., 1982. Metamorphic evidence for rapid (2 mm/yr) uplift of a portion of the Central Gneiss Complex, Coast Mountains, B.C. Canadian Mineralogy 20, 319–332.
Hollister, L.S., Crawford, M.L., 1986. Melt-enhanced deformation: a major tectonic process. Geology 14, 558–561.
Hutton, D.H.W., 1982. A method for the determination of the initial shapes of deformed xenoliths in granitoids. Tectonophysics 85, 45–50.
Hutton, D.H.W., 1988. Granite emplacement mechanisms and tectonic controls: inferences from deformation studies. Royal Society of Edinburgh, Earth Sciences Transactions 79, 245–255.
Ildefonse, B., Fernandez, A., 1988. Influence of the concentration of rigid markers in a viscous medium on the production of preferred orientations. An experimental contribution. 1. Non coaxial strain. Bulletin of the Geological Institute University of Uppsala 14, 55–60.
Irvine, T.N., Baragar, W.R.A., 1971. A guide to the chemical classification of the common volcanic rocks. Canadian Journal of Earth Sciences 8, 523–548.
Kruhl, J.H., 1996. Prism- and basis-parallel subgrain boundaries in quartz: a microstructural geothermobarometer. Journal of Metamorphic Geology 14, 581–589.
Kruhl, J.H., 1998. Prism- and basis-parallel subgrain boundaries in quartz: a microstructural geothermobarometer: Reply. Journal of Metamorphic Geology 16, 142–146.
Langone, A., 2007. Metamorphic evolution of Hercynian low-pressure metasediments in Sila (Calabria): P-T-t path of the Mandatoriccio Unit. Ph.D. Thesis, University of Bologna.
Lardeaux, J.M., Ledru, P., Daniel, I., Duchene, S., 2001. The Variscan French Massif Central—a new addition to the ultra-high pressure metamorphic 'club': exhumation processes and geodynamic consequences. Tectonophysics 332, 143–167.
Ledru, P., Courrioux, G., Dallain, C., Lardeaux, J.M., Montel, J.M., Vanderhaeghe, O., Vitel, G., 2001. The Velay dome (French Massif Central): melt generation and granite emplacement during orogenic evolution. Tectonophysics 342, 207–237.
Lioy, P., 2006. Analisi petrografica, strutturale e geochimica delle rocce granitoidi di Mesoraca (Sila Piccola). Diplom. Thesis, Università della Basilicata.
Lorenzoni, S., Zanettin Lorenzoni, E., 1983. Note illustrative alla carta geologica della Sila alla scala 1:200.000. Memorie della Società Geologica Italiana 36, 317–342.
Matte, P., 1986. Tectonics and plate tectonics model for the Variscan belt of Europe. Tectonophysics 126, 309–339.
Matte, P., 2001. The Variscan collage and orogeny (480–290 Ma) and the tectonic definition of the Armorica microplate: a review. Terra Nova 13, 122–128.
Neves, S.P., Vauchez, A., 1995. Successive mixing and mingling of magmas in a plutonic complex of Northeast Brazil. Lithos 34, 275–299.
Neves, S.P., Vauchez, A., Archanjo, C.J., 1996. Shear zone-controlled magma emplacement or magma-assisted nucleation of shear zones? Insights from northeast Brazil. Tectonophysics 262, 349–364.
Paterson, S.R., Fowler, T.K., Schmidt, K.L., Yoshinobu, A.S., Yuan, E.S., Miller, R.B., 1998. Interpreting magmatic fabric in plutons. Lithos 44, 53–82.
Paterson, S.R., Vernon, R.H., Tobisch, O.T., 1989. A review of criteria for the identification of magmatic and tectonic foliations in granitoids. Journal of Structural Geology 11, 349–363.
Paterson, R.S., Pignotta, G.S., Vernon, R.H., 2004. The significance of microgranitoid enclave shapes and orientations. Journal of Structural Geology 26, 1465–1481.
Platt, J.P., Compagnoni, R., 1990. Alpine ductile deformation and metamorphism in a Calabrian Basement nappe (Aspromonte, south Italy). Eclogae Geologicae Helvetiae 83, 41–58.
Rottura, A., Bargossi, M.G., Caironi, V., Del Moro, A., Maccarrone, E., Macera, P., Paglionico, A., Petrini, R., Piccarreta, G., Poli, G., 1990. Petrogenesis of contrasting Hercynian granitoids from the Calabrian Arc, southern Italy. Lithos 24, 97–119.
Schenk, V., 1980. U-Pb and Rb-Sr radiometric dates and their correlation with metamorphic events in the granulite-facies basement of the Serre, southern Calabria (Italy). Contributions to Mineralogy and Petrology 73, 23–38.
Schenk, V., 1984. Petrology of felsic granulites, metapelites metabasics, ultramafics, and metacarbonates from southern Calabria (Italy): prograde metamorphism, uplift and cooling of a former lower crust. Journal of Petrology 25, 255–298.
Schenk, V., 1989. P-T-t paths of the lower crust in the Hercynian fold belt of southern Calabria. In: Daly, J.S., Cliff, R.A., Yardley, B.W.D. (Eds.), Evolution of Metamorphic Belts. Geological Society of London, Special Publication 43, pp. 337–342.
Schenk, V., 1990. The exposed crustal cross section of southern Calabria, Italy: structure and evolution of a segment of Hercynian crust. In: Salisbury, M.H., Fountain, D.M. (Eds.), Exposed Cross-Sections of the Continental Crust. Kluwer, Dordrecht, pp. 21–42.
Schmid, S.M., Casey, M., 1986. Complete fabric analysis of some commonly observed quartz *c*-axis patterns. American Geophysical Union Monograph 36, 263–286.
Spanner, B.G., Kruhl, J.H., 2002. Syntectonic granites in thrust and strike-slip regimes: the history of the Carmo and Cindacta plutons (southern eastern Brazil). Journal of South American Earth Sciences 15, 431–444.
Stipp, M., Stünitz, H., Heilbronner, R., Schmid, S.M., 2002. The eastern Tonale fault zone: a "natural laboratory" for crystal plastic deformation of quartz over a temperature range from 250 to 700 °C. Journal of Structural Geology 24, 1861–1884.
Stampfli, G.M., Borel, G.D., 2002. A plate tectonic model for the Paleozoic and Mesozoic constrained by dynamic plate boundaries and restored synthetic oceanic isochrons. Earth Planetary Science Letters 196, 17–33.
Thomson, S.N., 1994. Fission track analysis of the crystalline basement rocks of the Calabrian Arc, southern Italy: evidence of Oligo-Miocene late-orogenic extension and erosion. Tectonophysics 238, 331–352.
Tiepolo, M., Bottazzi, P., Palenzona, M., Vannucci, R., 2003. A laser probe coupled with ICP Double-Focusing Sector-Field mass spectrometer from in situ analysis of geological samples and U-Pb dating of zircon. The Canadian Mineralogist 41, 259–272.
Tobisch, O.T., McNulty, B.A., Vernon, R.H., 1997. Microgranitoid enclave swarms in granitic plutons, central Sierra Nevada, California. Lithos 40, 321–339.
Tribe, I.R., D'Lemos, R.S., 1996. Significance of a hiatus in down-temperature fabric development within syn-tectonic quartz diorite complexes, Channel Islands, UK. Journal of the Geological Society of London 153, 127–138.
Van Dijk, J.P., Bello, M., Brancaleoni, G.P., Cantarella, G., Costa, V., Frixa, A., Golfetto, F. , Merlini, S., Riva, M., Torricelli, S., Toscano, C., Zerilli, A., 2000. A regional structural model for the northern sector of the Calabrian Arc (southern Italy). Tectonophysics 324, 267–320.
Vernon, R.H., 2000. Review of microstructural evidence of magmatic and solid-state flow. Electronic Geosciences 5, 2.
Vernon, R.H., Johnson, S.E., Melis, E.A., 2004. Emplacement-related microstructures in the margin of a deformed pluton: the San José tonalite, Baja California, México. Journal of Structural Geology 26, 1867–1884.
Von Raumer, J.F., Stampfli, G.M., Borel, G., Bussy, F., 2002. Organization of pre-Variscan basement areas at the north Gondwanan margin. International Journal of Earth Sciences 91, 35–52.
Wagner, G.A., Reimer, G.M., Jäger, E., 1977. Cooling ages derived by apatite fission track, mica Rb-Sr and K-Ar dating: the uplift and cooling history of the Central Alps. Memorie dell'Istituto di Geologia e Mineralogia dell'Università di Padova 30, 1–27.
Wallis, G.J., Platt, J.P., Knott, S.D., 1993. Recognition of syn-convergence extension in accretionary wedges with examples from Calabrian Arc and eastern Alps. American Journal of Science 293, 463–495.
White, A.J.R., Chappell, B.W., 1988. Some supracrustal (S-type) granites of the Lachlan Fold Belt. Royal Society of Edinburgh, Earth Sciences Transactions 79, 169–181.
Wilson, M., 1993. Magmatism and the geodynamics of basin formation. Sedimentary Geology 86, 5–29.